The Radiation Source ELBE

At the Forschungszentrum Rossendorf (FZR) a major new installation is approaching its completion - the "Strahlungsquelle ELBE". This radiation source will use the high brilliance electron beam from a linac with superconducting rf-cavities to produce various secondary beams for experiments in nuclear, solid-state, environmental and bio-medical physics as well as in various other fields. To present a comprehensive status report of this important and innovative project, the present Annual Report combines contributions made to it by several groups and departments of the FZR. The Departments "Experimental Facilities and Information Technology" and "New Accelerators" as well as the ELBE-beam-diagnostics-group have carried out numerous developments within the ELBE project; the most important are described mainly in the beginning of this Report. The subsequent contributions from groups of the IKH are more strongly focused on the production and future use of the different kinds of secondary radiation.

Physics with IR-FEL's and their radiation

The high brilliance electron beam produced by a super-conducting linac like ELBE allows the investigation of various processes which produce high quality electromagnetic radiation in various energy (i.e.) ranges. An especially illustrative and theoretically clear example for the generation of radiation is the Free-Electron-Laser (FEL). With the electron energy range available at ELBE coherent infrared radiation from 300 μm (corresponding to 1 THz) to 3 μm (equivalent to 0.4 eV) can be produced in short pulses of a few ps and with a large repetition rate finally allowing tens of watts average intensity. At the long wavelength side the limitation results mainly from the difficulties in handling the strong diffraction effects. Various theoretical and numerical studies have been performed on this problem and on the resulting IR-beam properties; laboratory experiments to test some of these calculations are presently being set up. For the short wavelengths the quality of the electron pulses and the undulator field is crucial. Our newly perfected pulsed-wire field scan allows to cross-check the detailed field maps obtained with Hall-probes and it will be used to document 'in situ' future variations in magnetic field strength. Research making use of IR- radiation in the 10 μm-range has been performed at existing FEL facilities and with Fourier- transform (FTIR)-spectroscopy methods. A FTIR-spectrometer operable in conjunction with a reflection-optic microscope is newly available at the institute to be used in conjunction with the IR-studies on biomedical probes to be performed at the FEL in the next years by scientists from the IKH.

X-rays, Bremsstrahlung Photons and Neutrons

Quasi-monochromatic X-rays can be generated from the fast electrons either by using the channeling process in single crystals (esp. diamond) or by Compton scattering of intense laser light from the electrons. For both processes a very high brilliance e-beam has to be realized which requires a beam transport system allowing for the reduction of unwanted emittance growth effects. At ELBE a decrease of the transverse emittance beyond present values is expected from improvements of the e-gun and finally the use of a photo cathode gun directly coupled to a superconducting cavity. Space charge effects can be minimized by enlarging the repetition rate from 13 up to 260 MHz - at constant average beam intensity. Studies will be performed to enhance the yield of channeling X-rays by resonant variation of the crystal parameters using a variable frequency ultra-sound field; additionally an improvement of the X-ray-to-bremsstrahlung-ratio will be strived for by inserting polycristalline carbon segments between radiator and probe. To promote the radiation damage studies planned by the IKH for the X-ray beam a cell-laboratory has *been set up in the ELBE building.*

In the case of MeV-bremsstrahlung to be used for nuclear spectroscopy a reduction of the background seen by the high resolution Ge-detectors will be aimed for by installing: (a) a vacuum tube to transport the beam from the radiator to the nuclear target, (b) a graded collimator made from pure Al, a material with low neutron production yield, (c) an extended photon beam stop formed by a hydrocarbon surrounded by Pb, (d) anti-coincidence shields from BGO around the detectors and (e) a coincidence circuit suppressing radiation delayed with respect to the e-bunches. First experiments on this beam-line will study the dipolar response of Mo-nuclei to photons of 5 to 15 MeV in dependence of their neutron number. Even more neutron-rich isotopes in this mass range will be accessible for spectroscopy as products from photon-induced fission in the future; such studies also deliver information of importance for the detailed understanding of the stellar synthesis of the heavier chemical elements.

The fast neutrons produced from the ps-e-bunches available at ELBE can be tagged such that a rather good energy resolution is obtained already after a few meter of flight path. The research envisaged here includes the investigation of fast neutrons with matter, especially with material for or from fission or fusion reactors. Also novel studies in the field of nuclear spectroscopy or nuclear astrophysics may become possible.

Collaborations

Within the FZR a close collaboration was established with the two departments responsible for the installation and operation of ELBE (i.e. Experimental Facilities / Information Technology and New Accelerators / ELBE-beam-transport and -diagnostics). Intense contacts also exist with the other Rossendorf institutes planning to use ELBE:
1) The Institute of Ion Beam Physics & Materials Research and the IKH are jointly installing equipment in the optics laboratories including a fs-laser system which will be synchronized to the ELBE e-bunches thus allowing studies of the temporal e-bunch structure as well as investigations of ultra-fast processes involving IR-pulses from the FEL.
2) The Institute of Radiochemistry and the IKH are jointly working on improving the sensitivity of IR-spectroscopical methods by replacing conventional thermal sources by the intense FEL- radiation; first exploratory studies in this field have been started at the CLIO-FEL at Orsay.
3) The Institute of Safety Research has joined the DFG-project on the "Interaction of fast neutrons with matter, esp. with materials for and from fusion and fission reactors", which also includes groups from IKH as well as from Dresden University.
Various collaborative efforts have been or are being formed to make use of the various novel research possibilities offered by ELBE and its secondary beams. As a typical example the EU-project THz-Bridge is mentioned here; it brings together scientists from IKH, from Frankfurt and Stuttgart universities and from four other EU-countries in a study on the interaction of far-IR and THz radiation with living cells.

Optimization of Transverse Emittance of the Thermionic Injector at ELBE

P. Michel, A. Büchner, P. Evtushenko, K. Möller, C. Schneider, J. Teichert

The injector concept for ELBE

To meet the different electron beam requirements according to the concept of ELBE to produce a wide range of radiation (Infrared radiation from FEL's, MeV-bremsstrahlung, X-rays, neutrons) an injector with optimum parameters for all these applications and easily changeable operation modes is needed. For example: to drive the FEL an electron beam with fixed repetition rate (13 MHz) at maximum peak current is necessary whereas for producing X-rays as channeling radiation the transverse emittance should be as low as possible (< 2 mm mrad, rms). To make Time-of-Flight experiments with neutrons the pulse to pulse distance should be variable up to micro seconds. These demands are well accomplished by an electronically grid-pulsed thermionic gun [1], which can be operated with variable frequency and bunch charge. A macro pulser based on a circular magnetic bending system interrupts the beam with adjustable duty cycle and allows a very flexible time structure of the beam. The gun is operated at 250 kV. Bunch compression is done by two bunchers operating at 260 MHz and 1.3 GHz, respectively. At two locations in the injector beam line insertable apertures are installed with three different diameters to optimize beam size and transverse emittance. The described injector set up is shown in Fig. 1.

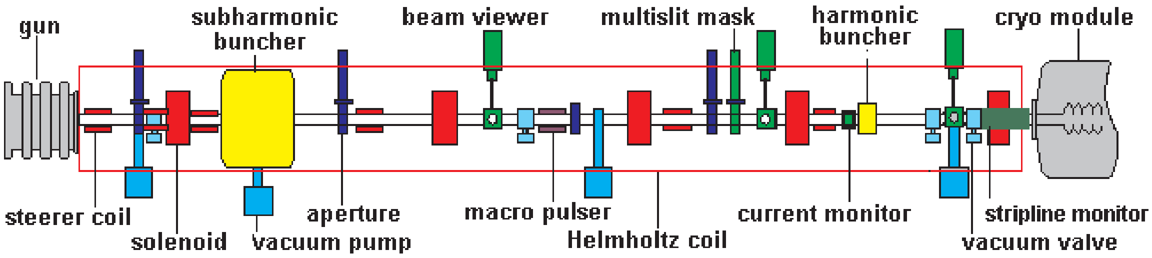

Fig. 1 *Set up of the thermionic ELBE injector*

Transverse emittance measurement

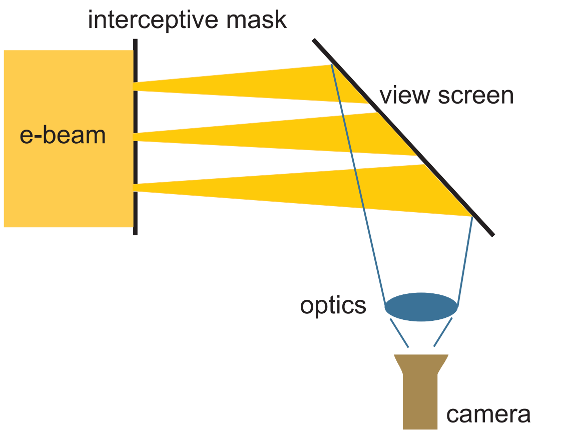

Fig. 2 *Multislit set up for transverse emittance measurement*

The electron beam from the gun and bunching stage (injector) was studied using a diagnostic module (Fig. 2). A multislit mask and a beam viewer allow to measure the transverse emittance in the range from 1 to 20 mm mrad with two different mask geometries. Fig. 3 shows the measured transverse geometric emittance of the ELBE injector at 13 MHz and 260 MHz pulse repetition rates. The 260 MHz regime allows operation at very low bunch charges which is important to achieve low emittance values. For comparison, Fig. 3 presents the results of a numerical simulation, too [2]. It can be seen that in the FEL mode the transverse emittance only slightly exceeds 13 mm mrad, which is sufficient to produce IR radiation down to a few microns. For Radiation Physics the emittance requirements can be met by increasing the repetition rate up to 260 MHz and reducing the transverse phase space by two apertures.

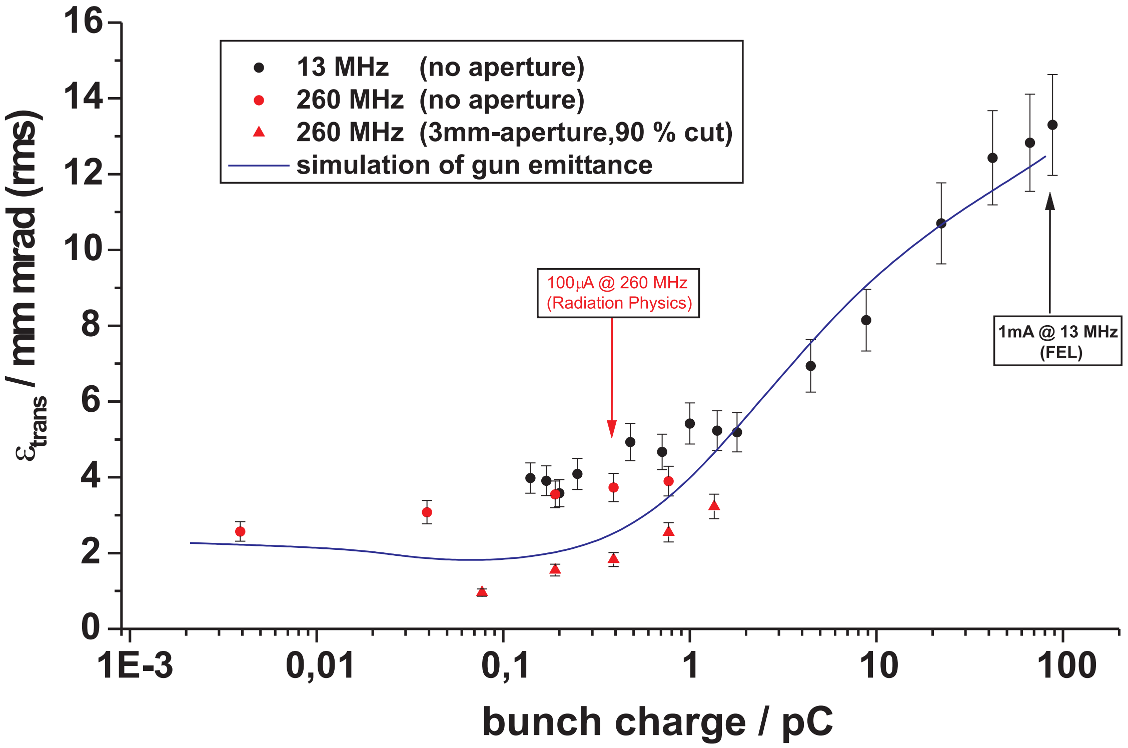

Fig. 3 *Transverse emittance of the thermionic ELBE injector*

References

[1] ELBE Design Report, FZR (1998)
[2] J. Teichert, this Report

Computation of the Transverse Emittance of a Thermionic Electron Gun Including Control Grid Effects

J. Teichert, P. Michel

Recently the injector beam parameters of the superconducting electron linear accelerator [1] were measured. For the transverse emittance an increase with bunch charge was found [2]. It grows from about 2 mm mrad for low bunch charges to nearly 14 mm mrad at a bunch charge of 85 pC. More detailed studies showed that this behaviour was rather independent of the injector operating parameters (bunching, pulse repetition rate) and that the emittance growth already takes place in the electron gun. The electron gun is a thermionic triode type with 250 kV cathode voltage and two-step acceleration. The gun has a cathode of 8 mm diameter and a 200 μm grid about 150 μm in front of it. By means of the grid, electron pulses are formed with either 13 or 260 MHz and a pulse length of about 600 ps. The maximum peak current is 140 mA which corresponds to a bunch charge of 77 pC and an averaged current of 1 mA at 13 MHz.

Numerical simulations were performed in order to understand the increase of the transverse emittance with bunch charge. Possible reasons which may cause the emittance growth and are considered within the simulations are: the thermal energy spread of the electrons, influence of the electrostatic accelerating field formed by the electrodes (geometrical aberrations), space charge effects, and the influence of the control mesh. For the calculations the program EGUN [2] was used.

As an example of the electrode geometry effect, Fig. 1 shows the influence of the Pierce electrode angle on the transverse emittance. It can be seen that the emittance decreases if the angle is increased. But this result is independent of the bunch charge and the emittance values are always much lower than the measured ones. The space charge effect is presented in Fig. 2 which shows the transverse emittance as function of the peak electron current. A significant effect on the transverse emittance is found for peak currents higher than about 1 A.

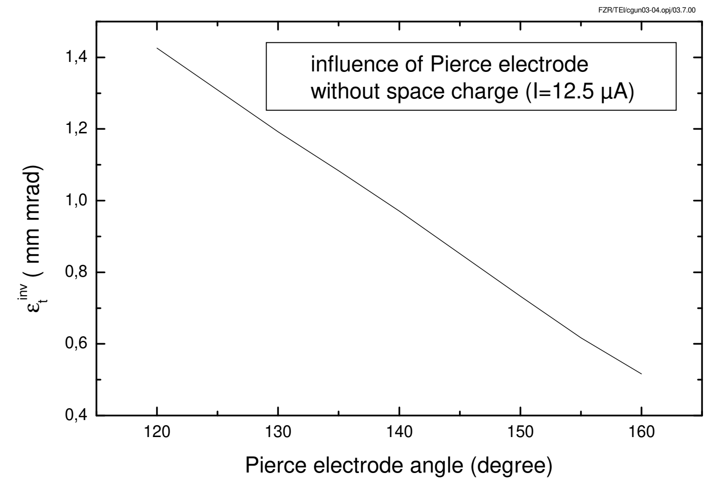

Fig. 1 *Transverse emittance (RMS) as a function of Pierce electrode angle.*

The control grid is a source of emittance growth because the strong acceleration field penetrates through the mesh holes, and for the electrons each hole acts as a lens. In order to estimate this effect a formula was derived by Reiser [4]. But this formula cannot be applied in the present case where the mesh is always on negative potential. Therefore the grid effect was studied numerically by modifying the GUN code. For the electron transmission through the potential barrier of the mesh the free electron gas approximation with a local penetration probability , a Maxwell energy distribution, and Lambert's law were applied. Although the model is rather simple and stationary calculation with circular mesh holes are performed, the experimental results are well described by the calculation, as can be seen in Fig. 3. Thus, it can be assumed that the emittance growth is mainly caused by the grid. Furthermore the computer simulation predicts that smaller transverse emittance can be obtained at the ELBE injector by means of a smaller cathode diameter or/and a finer control mesh.

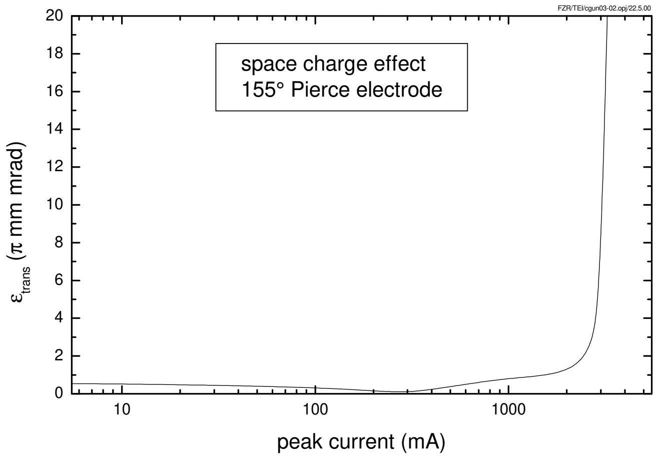

Fig. 2 *Transverse emittance (RMS) as a function of peak current (space charge effect).*

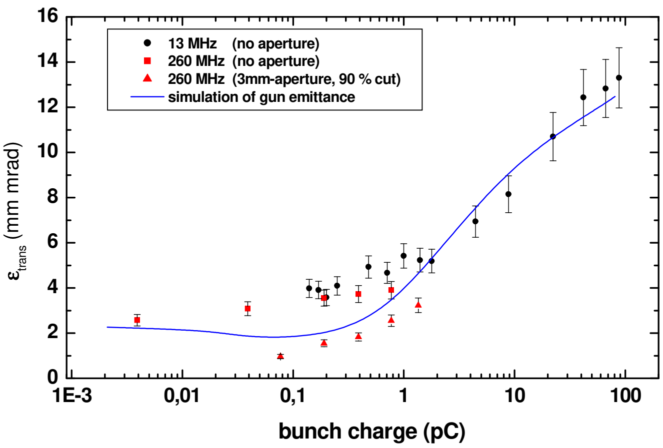

Fig. 3 *Transverse emittance (RMS) as a function of bunch charge measured at the ELBE injector for 13 and 260 MHz pulse repetition rate and with an additional aperture. The curve presents the calculation result of the grid effect.*

References

[1] F. Gabriel et al., Nucl. Instr. Meth. B 161-163 (2000) 1143
[2] P. Michel, this Report
[3] W.B. Hermannsfeldt, Report SLAC-331-UC-28, Stanford University, 1988
[4] M. Reiser, Theory and Design of Charged Particle Beams, Wiley, New York, 1994, p. 97

Status of the Superconducting RF Gun

D. Janssen

The development of a superconducting RF photocathode gun (SRF gun) is under way. SRF guns are the most advanced type of electron injectors, which combine high brightness and large bunch charges of normal conducting RF guns with the cw-mode and large average current of superconducting cavities. Numerical calculations of beam parameters for this gun show excellent results [1]. In the framework of the ELBE project we need this gun for the following reasons:
The minimal lenghts of the electron bunch, which can be obtained by this gun is smaller than 100 μm. This leads for an average electron current of 1 mA to a coherent undulator radiation in the order of 1 W with a wave lengths of 100 μm [2]. In this way for wavelengths $\lambda \geq 100\,\mu$m the SRF gun allows the generation of an intense, coherent infrared light without the optical resonator, used in the FEL.
In order to obtain intense and monochromatic radiation in the X-ray region with an electron beam energy equal or less than 40 MeV (which is the maximal energy of the accelerator), in the framework of the ELBE project different methods are planned and under discussion. In all of these methods (channeling radiation, transition radiation, parametric X-rays, Compton back scattering) the radiation output increases with decreasing of transversal emittance. Furthermore, the output of the Compton backscattering increases with increasing bunch charge. The SRF gun provides for a given bunch charge essential lower transversal emittances than the conventional injector, which is installed in the first phase of the ELBE project [1].
In the ELBE project time-of-flight measurements of fast neutrons for experiments in astrophysics, nuclear physics and for transmutation experiments are planned. For these measurements a point like neutron source with intense neutron pulses and variable time structure is necessary. These neutron pulses can be obtained by the interaction of an electron bunch with a target, where the electron bunch has the same properties as one expects for the neutron pulse. So for these experiments an electron beam with large bunch charge, small emittance and variable time structure is necessary. The possibility to create such an electron beam is one of the advantages of the SRF gun [1].
The design of the SRF gun is described in [3]. The status of its five parts is the following:

1. The main part is the cryostat with the gun cavity, the RF input coupler and the tuning mechanics for the cavity.
   The cryostat has been assembled and vacuum tested. The gun cavity has been prepared in the clean room of DESY. In a test cryostat excellent values for the maximal electric field and the Q-value were measured, see Fig. 1 and [3]. Also at DESY the cavity has been assembled together with the neighbouring beam tubes, with the coupler and with the cathode insertion device. All these parts are now installed in the cryostat at Rossendorf.

2. The photocathode preparation chamber together with the transfer tube for the photocathodes have been build and tested. In this chamber first $TeCs_2$ photolayers have been prepared. The mechanical transfer of the cathodes under vacuum from the chamber into the gun cavity inside the cryostat have also been checked.

3. The beam diagnostic module contains a viewscreen and a beamdump at the end, where beam of 2 kW can be absorbed. It has been assembled and vacuum tested. We are able to measure the beam profile and the current.

4. The fourth part is a mode locked UV laser together with a optical transfer line from the laser table to the photocathode inside the cavity. A first version of the laser has been developed at the Max Born Institute in Berlin.

5. The RF power supply together with the wave guide to the RF coupler and the control panel have been installed and tested.

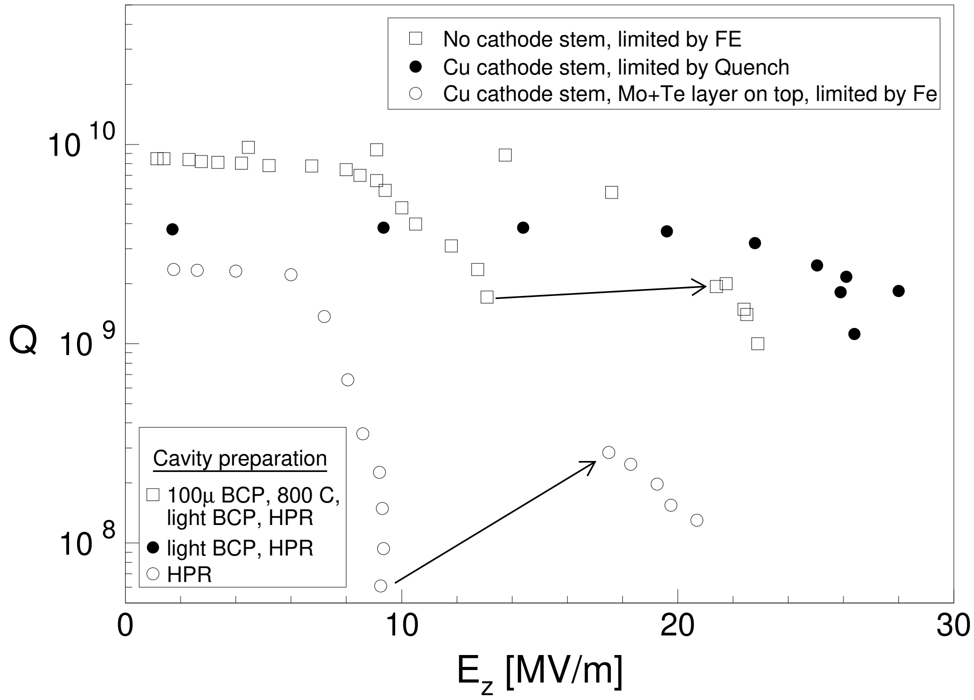

Fig. 1 *Results of the Vertical Cavity Tests obtained at a liquid Helium temperature of 2 K.*

References

[1] D. Janssen, V. Volkov
RF - focusing, an instrument for beam quality improvement in superconducting RF guns
Nucl. Instr. Meth. A 452 (2000) 34-43

[2] V. Volkov, D. Janssen, R. Wünsch
Generation of sub-picosecond electron bunches from superconducting 3+1/2 cell gun
Submitted to PAC 2001, Chicago

[3] E. Barthels et al.
On the way to a superconducting RF - gun, Nucl. Instrum. Meth. A 445 (2000) 408-412

Electron Beam Diagnostics at ELBE

A. Büchner, P. Evtushenko, U. Lehnert, P. Michel, K. Möller,
C. Schneider, J. Teichert

To optimize and control the electron beam at the ELBE facility a comprehensive system of diagnostics has to be provided similar to other facilities such as CEBAF, TTF, S-DALINAC or MAMI. In general there are two types of diagnostics. For destructive diagnostics a special diagnostics mode of beam operation was defined in order to limit the dissipated beam power. Nondestructive diagnostics can be used at all times to monitor the full-power operation of the beam. The system of diagnostics at ELBE will contain the following components:

Beam viewers

The beam viewers are operated in the diagnostics mode at an average beam current of about 1 μA and nominal bunch charge. The beam current is then controlled by the macro pulse parameters. The beam viewers are used to adjust the beam by optical inspection of the position and the size of the beam spot. Beam profiles can be determined using image analyzing software. In energy dispersive regions of the beamline viewers can be applied to measure the energy spread. In connection with multi slit masks or quadrupoles the transverse emittance of the beam can be measured. The described beam viewer concept was succesfully tested at the injector using the following equipment: screens – 500 μm Al_2O_3 ceramic (fluorescence) or 8 μm Al foil (OTR), cameras – Vidicon KH500 with Saticon tube XQ1300SF (radiation resistant), in some cases CCD cameras KAM02E, external target illumination, video multiplexing system (remote control) and a PCI-1407 frame grabber board which delivers at maximum 25 images/s synchronized to the macropulse.

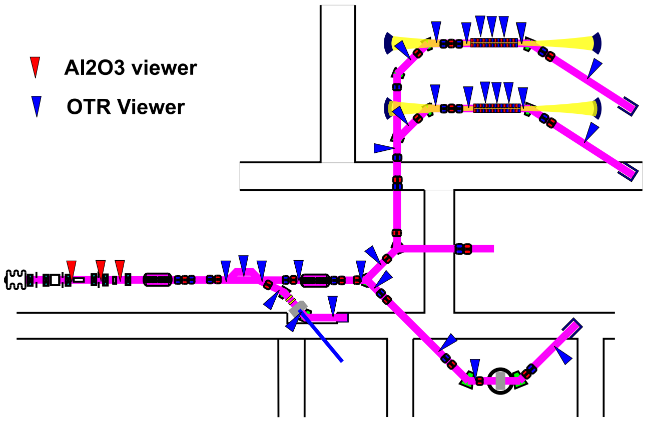

Fig. 1 *ELBE beam viewers*

Beam position and beam current monitors

These monitors are realized as strip line monitors with the following details: 35 mm diameter, signal filter 1.3 GHz with 60 MHz band width, signal conversion using an AD 8313 logarithmic rms-to-DC converter chip (0.1 - 2.5 GHz; 70 dB) into a 12(16) bit ADC. One prototype of the proposed strip line monitor was tested at the injector. A spatial resolution of < 30 μm was achieved in the current range of 10 - 1000 μA. The analysis of the strip line monitor signal with respect to its time behaviour allows the measurement of the bunch length with time resolution < 100 ps. Thereby the strip line monitors can be used for optimization of the bunch compression in the injector to deliver an optimized beam to the accelerator section. Additionally to the strip line monitors information on the beam current can

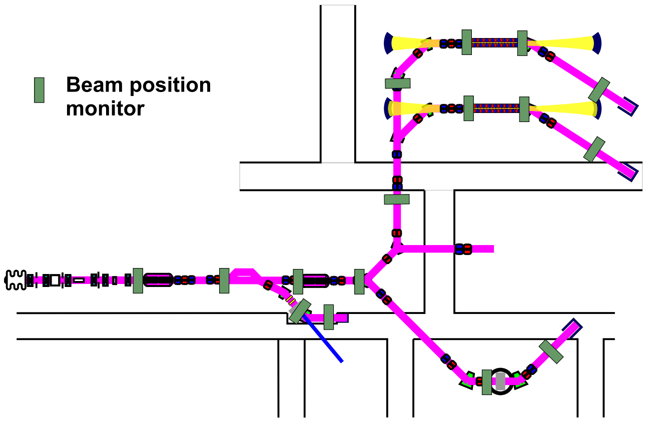

Fig. 2 *ELBE beam position monitors*

also be obtained at the various apertures and wall current monitors and at the beam dump.

Martin-Puplett Interferometer (DESY-design)

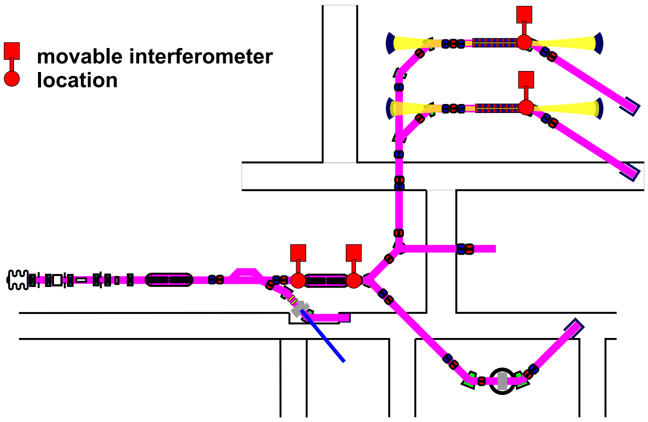

Fig. 3 *ELBE bunch length measurement*

The interferometer serves for measuring the bunch length in the submillimeter range by measuring the autocorrelation function of the coherent transition radiation. Golay cells are used to register IR radiation, the bunch length is calculated by the Kramers-Kronig method. The assembly of the interferometer is finished. At present the software for analysis is being developed.

Beam loss monitors

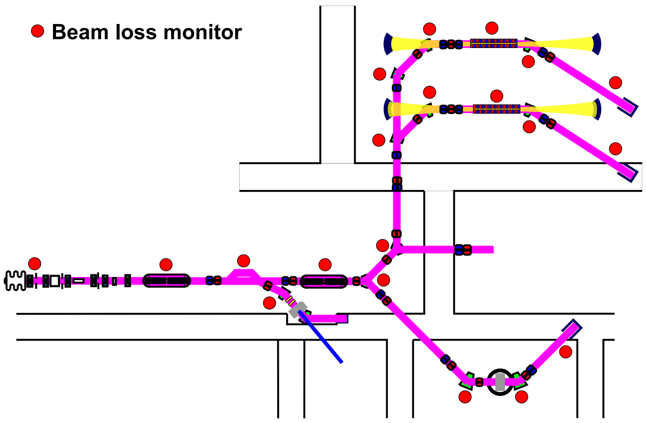

Fig. 4 *ELBE beam loss monitors*

The aim of these monitors is to measure the beam loss at a number of positions to ensure full beam transmission and to have some protection against thermal and radiation damages. They consist of „low cost“ photomultipliers (EMI9125) measuring bremsstrahlung radiation produced by electrons striking the beam tube and a count-rate integrator using VC 110 f/V-converter chips that deliver a radiation-dose signal into an ADC input. An optical test pulse will be used to ensure fail-safe operation. During tests at the injector this simple concept turned out to be fully efficient delivering signals proportional to the radiation dose.

Status of the Stripline Beam Position Monitors System at ELBE

P. Evtushenko, A. Büchner, K. Jordan[1], P. Michel

The ELBE accelerator needs a system to monitor the electron beam position in full power mode. The system will be used for optimization of the electron beam transport in the accelerator and for control of the electron beam position at the targets. The system must be nondestructive and should not affect the electron beam quality. Required resolution is about 100 μm for ± 5 mm from center. For this reason a system of stripline beam position monitors (BPM) is under design. The stripline BPM is a nondestructive device with negligible influence on the beam behavior. It is known that with stripline BPMs one can easily achieve a resolution considerably smaller than 100 μm.

To verify the basic principles of the stripline BPM and to get information about the BPMs signal behavior we did a set of measurements on the ELBE injector with a CEBAF FEL stripline BPM. We have to note that the CEBAF BPM was build for an accelerator with the fundamental frequency 1.5 GHz (as compared to 1.3 GHz at ELBE) and another beam pipe diameter. So this BPM has properties slightly different from BPM designed for ELBE. But nevertheless the general behavior of the BPM is the same and therefore the measurements were very useful for our understanding. The measurements were also necessary for the design of the BPM electronics. By means of a spectrum analyzer we measured the amplitude of the BPM signal at 1.5 GHz as a function of the beam current. The measurements gave the dynamic range of the signal which we have to take in to account in the electronic design. We also measured the amplitude of the signals from two opposite strips as a function of the beam position. The position of the beam was measured by a cromox viewscreen with a resolution much better than the BPM resolution. From this measurements we estimated the sensitivity and the achievable resolution of the BPMs.

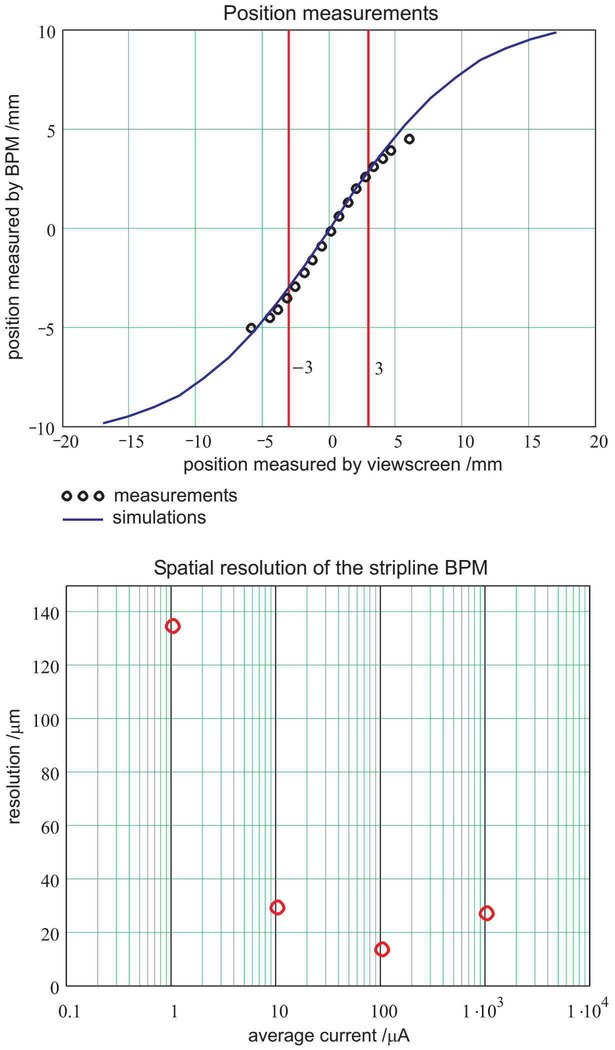

Fig. 1: *Calculated and measured response of the BPM (up), measured resolution (down).*

We also did simulations of the BPM signal behavior. The simulations were done by a simple Mathcad code. The code gives the capability to calculate the spectrum of the BPM signal as a function of bunch charge, bunch length and beam position. Here we present the results of the simulations together with results of the measurements as described above.

The measured sensitivity of the BPM is 243 mV/mm versus calculated 232 mV/mm such that there is a difference of 4.5 %. The deviation between measurements and simulation for the beam displacements of more than $3 \div 4$ mm is due to the fact that during the measurements the BPM was installed downstream of the dipole with relatively small gap (the electron beam was cut by the vacuum chamber in the dipole).

One of the BPMs will be installed downstream of the first cryomodule. The BPM will serve for measurements of the electron beam position at the entrance of the cryomodule and for setting the correct phase and power of both bunchers of the injector. The electron bunch from the injector must enter into the module in the accelerating phase of the RF field and must have minimal length. Since the power spectrum of the beam depends on the bunch length measurements in the frequency domain can give information about the bunch length and one thus gains important information to set the bunchers. To check this possibility we did two sets of measurements. By means of a spectrum analyzer we measured the power of the 1.5 GHz peak in the BPM signal spectrum with different settings of the first subharmonic buncher.

The maximum of the signal corresponds to the minimum of the bunch length. Thus the optimum settings of the subharmonic buncher are turned out to be 500 W power and 5^o phase.

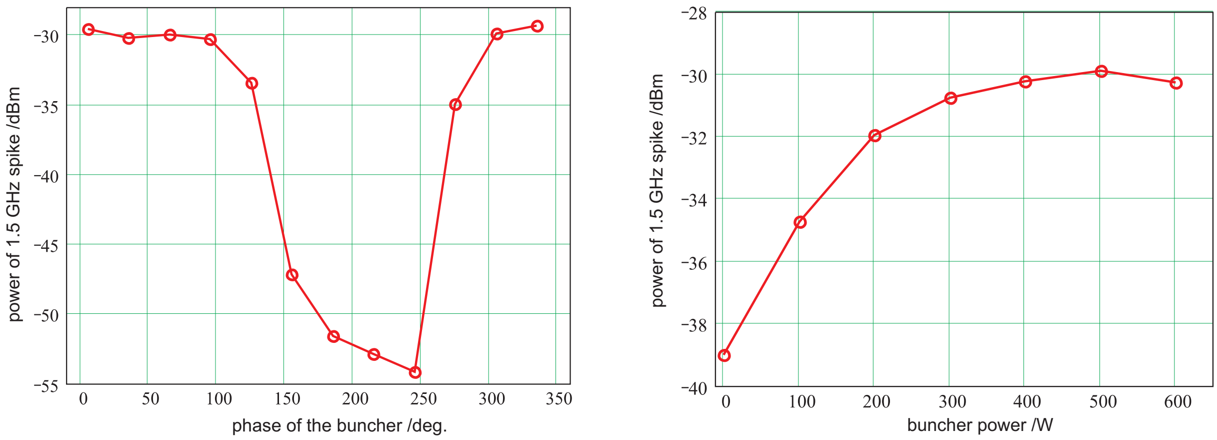

Fig. 2 *Measured power at 1.5 GHz with the following conditions: (left) dependence of the signal on the buncher phase with the power of the buncher set at 500 W; (right) dependence of the signal on the buncher power with the buncher phase constant at* 5^o*.*

[1] *Thomas Jefferson National Accelerator Facility, Newport News, Virginia 23606, USA*

Design of Electronics for the Stripline BPM

P. Evtushenko, A. Büttig, K. Jordan[1], P. Michel

The ELBE accelerator is operated with a time structure of the electron beam which is either cw or pulsed mode with a macropulse length down to 100 μs. Because of this time structure it is straightforward to use electronics operating in the frequency domain for the beam position monitors (BPM). The stripline BPM has a large bandwidth, at least 6 GHz, which we can see by means of a Network analyzer. The idea is to take a part of the BPM RF signal and to send it through electronics which will give a rms of the RF signal; in other words the electronics will convert the RF signal to DC with an amplitude proportional to the power of the RF signal. Microchips with 2.5 GHz bandwidth which can treat RF signals in this way are now available. There are two possible schemes of the BPM electronics under development. The first one is based on the logarithmic amplifier AD8313, the other one on the rms-responding true power detector AD8361. The features of the chips are shown in Fig.1.

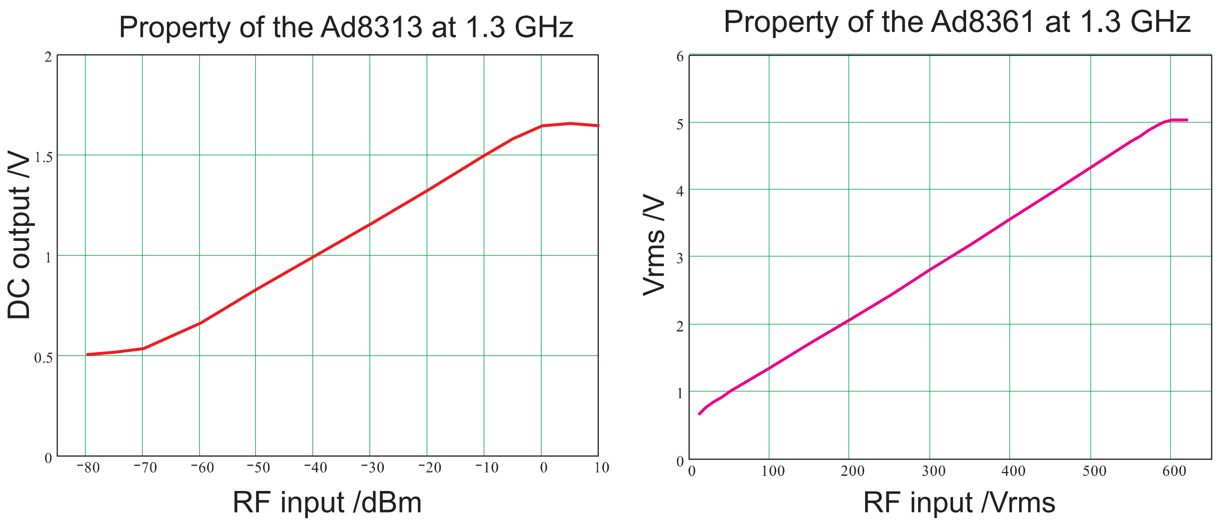

Fig. 1 *Characteristics of the chips which are used for the BPM electronics.*

The block-diagrams of the proposed electronics are given in Fig. 2.

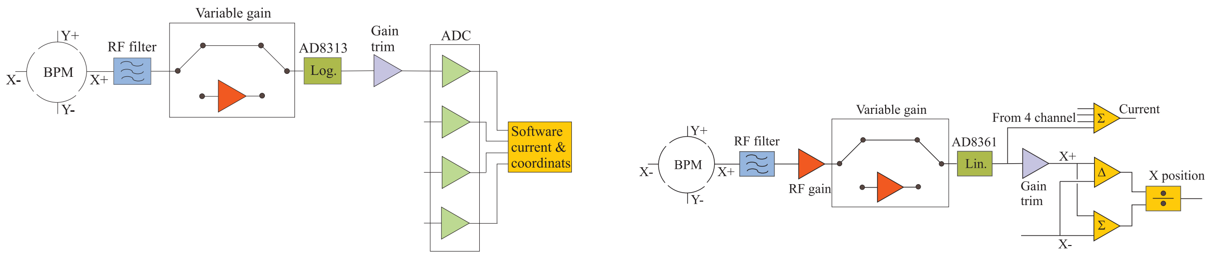

Fig. 2 *Proposed schemes of the BPM electronics, based on the logarithmic amplifier AD8313 (left) and on rms-responding true power detector AD8361(right).*

The electronics based on the AD8361 allows to calculate the electron beam position in an analog device and thus it can be more useful in time critical measurements. The scheme based on the logarithmic amplifier does not give such a possibility. In this case position and current will be calculated by software which results in a longer evaluation time. Such software for the BPM system was done in LabView.

[1] *Thomas Jefferson National Accelerator Facility, Newport News, Virginia 23606, USA*

Diagnostic Software at ELBE

Ch. Schneider

The control and data acquisition system of ELBE is a PC-based system using standard net technologies like e.g. OPC (Object Linking and Embeding (OLE) for Process Control) to interface the system components. The part of the system from which the diagnostics value are achieved is subdivided into two scopes of duties. The first is the section which acquires the raw data and processes the data (referred to as the DAQ/IMAQ). For this an example is: images from the beam distribution are grabbed from a VIDICON camera and vertical and horizontal profiles are extracted from the image data. The second is the section which processes the data in further steps to achieve more complex diagnostic variables and prepare indicators for the operator user interface (referred to as the diagnostic software). Whereas LabWindows is the development tool for the DAQ/IMAQ part for historical reasons, in general LabView will be used for the diagnostic software; it provides a well established link to LabWindows. The communication between these two system parts is realized through the DataSocket technology [1].

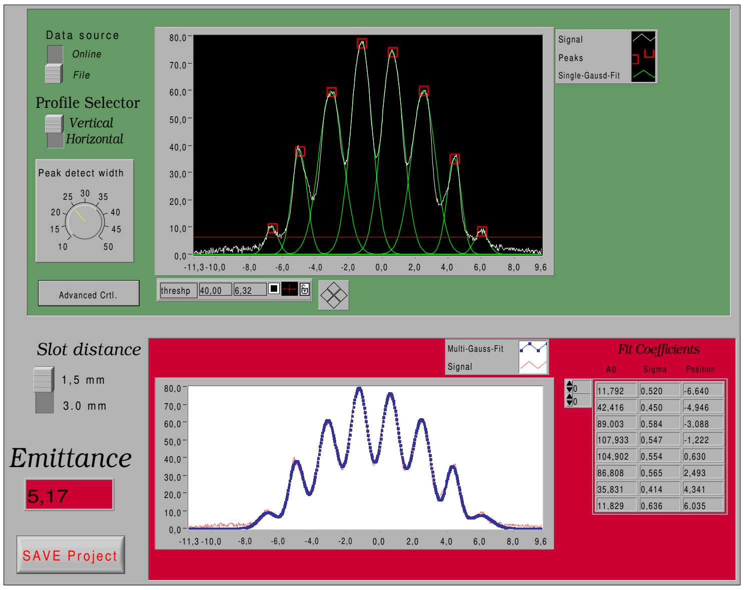

Fig. 1 *Tool to determine the emittance by the multi slit methode*

One of the important tasks in the diagnostic is the control of the beam emittance. This is done in the injector part of the accelerator with two methods. One is the multi slit method which demonstrates what kind of requirements the diagnostic software has to fulfil. In the multi slit method parts of the beam are cut out by a slit mask and are recorded from a detection screen with a camera. From the Image acquisition system IMAQ the profile data are sent to the diagnostic software. Here the image profile is fitted by a multi Gaussian function and the emittance is calculated from the fit parameters (see fig. 1).

Therefore the diagnostic software must provide complex signal analysing tools like the multi Gaussian fit and on the other hand support flexible operator controls and data indicators. In the tool displayed in fig. 1 it may be necessary to adapt the base line below the peaks or smooth the raw curve by an operator controlled width to find the correct number of peaks, which is a prerequisite for a successful multi Gaussian fit.

Unlike in other development tools a graphic programming language is used in LabView. The basic philosophy is to reflect the measurement hardware and signal acquisition in the software through the so-called (graphic) virtual instruments (VI). In that way it is consistent to reflect the diagnostic tasks like emittance, energy spread, beam profile, beam positions measurements and so on into single VIs. Since partly identical (e.g. read image profiles) subtasks have to be fulfilled much the same basic VI or subVI can be used in the program development. The data transfer between the VIs (like to the DAQ/IMAQ) is consequently realised with the DataSocket technology.

References

[1] http://www.ni.com/datasocket/wp1680.pdf

Beam Transport behind the LINAC 1

A. Büchner

The beam transport to the FELs has to perform a bunch compression and for that a chicane was planned between LINAC 1 and the „S“-arc. To design it the required transport matrix element R_{56} should be determined. This value depends on the longitudinal phase space after LINAC 1 and the desired longitudinal phase space in the FELs. Due to the complexity of the problem no exact values could be obtained from numerical simulations. As an estimate of the maximum required R_{56} a value of 450 mm was fixed. A variable chicane is planned which allows to vary R_{56} from 0 to this maximum. This gives an enormous flexibility in connection with LINAC 2, which for instance makes it possible to measure the longitudinal phase space.

To allow two-colour experiments at „ELBE“ with two FELs running synchronously in the future the beam transport has to be suitably designed. Even if these steps are not realized now the needed place for them has to be reserved. Because of tight space there is no other possibility than to combine the variable chicane with the beam separation for two-colour experiments and the beam transport to the nuclear physics experiments. A side effect of such a combination is the saving of extra dipoles for these tasks. As a consequence the size of the chicane is completely determined by the geometry resulting from the deflection angles of both energies at two-colour experiments. These angles were set to 30 and 45 degrees corresponding to a RF induced energy modulation of ± 5.23 MeV for a 30 MeV beam. This results in an even higher maximum R_{56} of the chicane of 633 mm with a maximum beam offset of 513 mm in its center. In Fig. 1 an overview of the chicane with the combined beam separation is given.

There exist five different beam paths in this design:

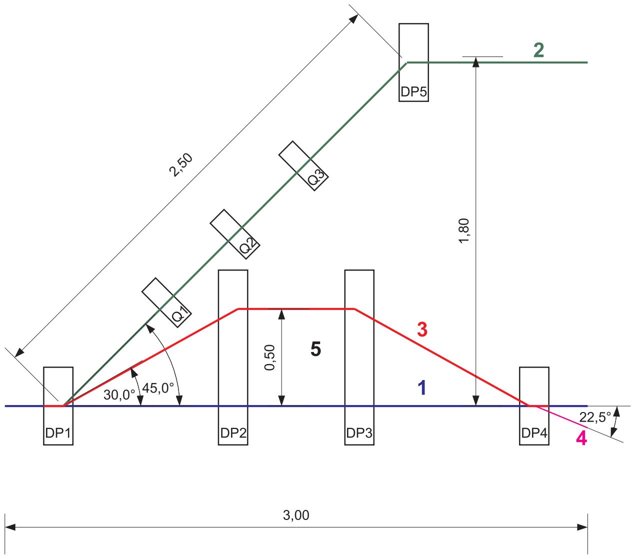

Fig. 1: *Design of beam separation combined with variable chicane*

- **1 -** Straight through to the radiation physics and neutron physics caves (all dipoles off).
- **2 -** A separate path for the beams with sufficiently low energy.
- **3 -** A path for the higher energy beam back to the continuation of line 1. For two-colour experiments this path and path 2 are used alternatively by subsequent pulses.
- **4 -** A beam path to the nuclear physics cave (only dipole 4 switched on).
- **5 -** A variable beam path for normal chicane operation.

Beam transport calculations for all five beam paths were performed and it is possible to match the beam to the different requirements. The position of the viewscreens and beam adjustment rules are defined.

Design of the Electron-Beam Transport to the ELBE Experimental Caves

U. Lehnert

For the FEL beamlines an S-shaped design with achromatic bends was chosen which performs a compression of the electron bunch on its way to the FEL undulators. Both bends of the S use a dipole-quadrupole-dipole layout. Position and focusing power of the quadrupoles have to be adjusted to achieve zero position and momentum dispersion. For the first bend this leads to an asymmetric quadrupole position, given the asymmetric pole-face angles of the used dipole magnets. For each bend a beam matching is possible which results in equal beam radii at the entrance and exit of the bend. Given the positions of the dipole magnets the phase shift in longitudinal phase space is fixed to R_{56}=93 mm. A preparation of a certain longitudinal phase-space correlation which leads to an upright phase-space ellipse at the undulator is done with a variable-R_{56} chicane in between the two accelerator cryomodules.

The straight beamline section between the bends is mainly determined by mechanical limitations as the beam has to go through a 2.4 m thick concrete wall in front of which a beam shutter is placed. Considering this, the quadrupole-doublet magnetic lens has to be placed inside the concrete wall immediately behind the shutter in order to limit the beam magnification. Including two single quadrupoles at the ends of the straight section an imaging of the matched beams of the bends onto each other is possible.

The undulator of the mid-infrared FEL consists of two 1 m long segments. Their spacing varies from 245 to 345 mm determined by the resonance condition between the optical and the electron beam. Due to the field-free drift space beween the undulator segments an ideal matching which would yield a constant-radius envelope is impossible. Instead, a symmetric matching condition was choosen which has a beam waist between the undulator segments. The beam diameter at the waist is determined as to produce minimal betatron oscillations and thus a minimal average beam diameter over the undulator. The beamline to the undulator contains a quadrupole triplet, which does not allow an ideal matching, as there are only three degrees of freedom for four matching conditions. However, there exist decent matching compromises for all possible undulator settings, yielding a reasonably small beam diameter in comparison to the optical beam.

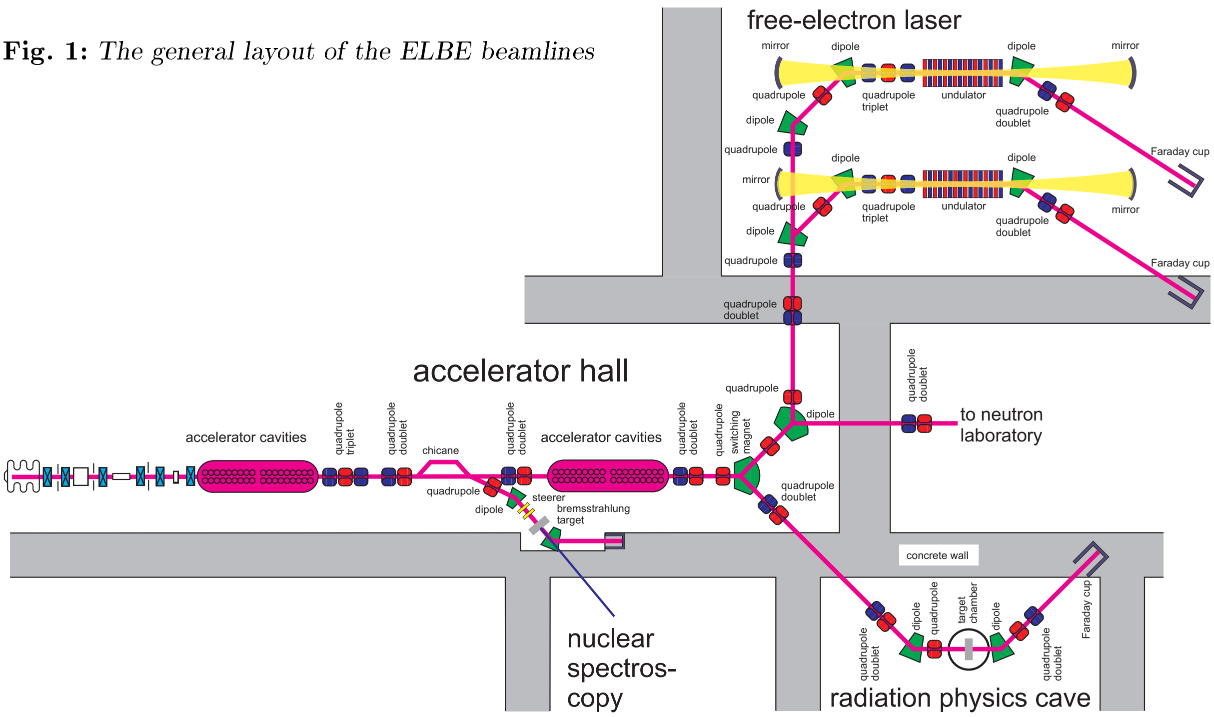

Fig. 1: *The general layout of the ELBE beamlines*

Space-charge effects on the electron beam transport were studied using the PARMELA [1] beam transport code. Electron beams which should allow an FEL operation can be supplied down to 10 MeV beam energy. The longitudinal phase shift R_{56} increases with decreasing energy from its design value R_{56}=93 mm at 20 MeV to R_{56}=160 mm at 10 MeV which has to be compensated for by tuning the chicane. At the same time, the longitudinal emittance and the energy spread of the beam are growing significantly. At 10 MeV the longitudinal emittance already triples but the beam quality still is just sufficient for the FEL operation.

The electron beam transport to the radiation physics cave has to be designed achromatic in order to conserve the low transverse emittance of the beam. This is achieved with a dispersion-crossover in the 45 deg section of the beamline. This crossover is placed asymmetrically in order to be situated outside the concrete wall and to be accessible for beam diagnostics. The necessary focussing is provided by quadrupole doublets before and after the wall that separates the accelerator hall from the radiation physics cave.
At the position of the channeling target a beam waist is created which diameter can be adapted to different experimental requirements. Either large focal spot sizes with very low beam divergence or rather narrow foci can be tuned using the two single quadrupoles situated before the switching magnet and after the first dipole in the radiation physics cave. The actual position of the focus is variable as well, thus allowing to use an alternative channeling target downstream the goniometer chamber, which design is optimized for the production of high-flux photon beams but lacks some of the flexibility of the goniometer.

For the nuclear physics beamline the last dipole magnet of the chicane is used in connection with one additional dipole and a quadrupole in between to achromatically deflect the electron beam by 45 degrees. A quadrupole doublet provides the necessary focusing onto the radiator target. A set of steerers is used to vary the angle of incidence of the electron beam with respect to the collimator axis, thus allowing experiments using partially polarized bremsstrahlung radiation emitted off the forward direction. The thickness of the radiator is limited by electron scattering and the according radiation background from electrons hitting the tubing. Therefore, special attention has to be paid to the design of the beam path from the radiator target to the beam dump, which has to be as short as possible and well shielded.

References
[1] L.M. Young, J.H. Billen, Los Alamos National Laboratory, LA-UR-96-1835

Measurements of the Electron Beam Profile and Position Inside Undulator by means of a Moveable YAG Screen

P. Evtushenko, P. Michel

Motivation

For operation of an FEL the overlap of the electron beam and the optical beam inside an undulator must be maximized. Both of them must be located in the magnetic axis of the undulator. To realize this one must be able to measure the electron beam position and profile inside the undulator with an accuracy of about 100 μm. These requirements are connected to the size of the electron beam and the optical mode in the undulator.

Scheme of the diagnostic system

The proposed diagnostics is shown on Fig 1. The system works in the following way: a moveable screen travels in the vacuum chamber which is located in the undulator. The travel length of the screen in the case of the undulator U27 is the length of the undulator (2×98 cm) plus a gap between the two parts of the undulator (~ 30 cm). In the case of undulator U50 the travel length is approximately the length of the undulator (~ 225 cm). That means the travel length of the screen is approximately the same for both undulators.

When the electron beam hits the YAG screen radiation with maximum intensity at 550 nm is produced. Downstream of the undulator there is a dipole magnet to bend the electron beam. The distance between the undulator and the dipole is approximately 140 cm. An insertable mirror is located behind the dipole. The mirror is used to deflect the YAG radiation from the vacuum chamber though a vacuum window. Near the vacuum window a lens is placed for imaging the screen to a CCD chip. Since the screen is moveable and we need to keep the optical path length between the screen and the lens constant we have to insert an element which has a variable optical path length. We can use a moveable roof mirror plus two mirrors 2 and 3, see Fig 1. The travel length of the roof mirror is half of the screen travel length. The mirror 4 and a very sensitive cooled CCD camera are located on the floor. The camera has to be shielded by a lead housing.

Choice of the screen material

As also hard X-rays will be produced, when the electron beam strikes the screen, the undulator magnets may loose magnetic strength in this high radiation environment; thus the screen should be as thin as possible. From this point of view an OTR screen would be preferable, since it is possible to make such screen from aluminium foil as thin as 10 μm. But in diagnostic mode with average current about 1 μA at an electron beam energy of 15 MeV $\div$ 40 MeV the radiation level in our collection solid angle is too small. Thus using an OTR is not sufficient for this diagnostic. The YAG crystal is a good alternative to the OTR screen in this case. Direct comparisons of the effective conversion efficiency, spatial resolution, and time response of the screens have been performed [1,2]. The light intensity of the YAG crystal is about 1000 times larger than with the OTR screen. A beam size growth has been observed for the YAG data relative to the OTR data above average current 60 mA. The fluorescence time of a the crystal has been measured [2]. The light intensity decay time was measured to be about 80 ns. YAG crystals with thickness 0.1 mm are commercially available [3].

The cooled CCD ST-237 [4] was chosen for the diagnostic, since it is sensitive enough and still not too expensive.

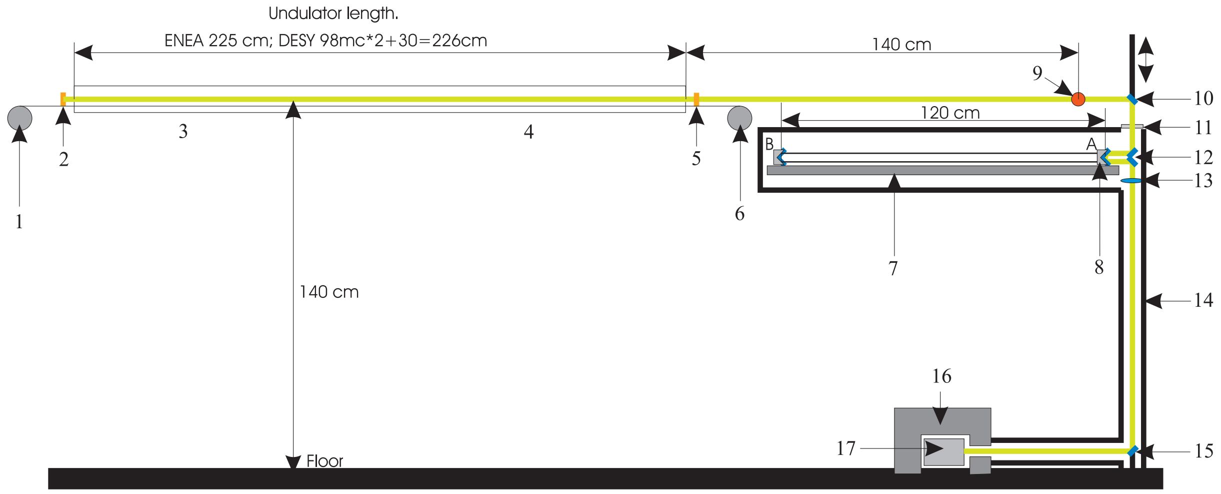

Fig. 1 *Scheme of the diagnostics. 1 - stepmotor 1, 2 - screen in position A, 3 - first part of the undulator U27, 4 - second moveable part of the undulator, 5 - screen in position B, 6 - stepmotor 2, 7 - linear motor stage with travel length 1.3 m, 8 - roof mirror on position A, 9 - position of the dipole, 10 - insertable mirror, 11 - window, 12 - mirrors, 13 - lens, 14 - light shielding, 15 - mirror, 16 - lead shielding, 17 - CCD camera.*

References

[1] A.H. Lumpkin, Nucl. Instr. and Meth. A 429 (1999) 336-340
[2] W.S. Graves, E.D. Johnson, A high resolution electron beam profile monitor, Proc. of Particle Accelerator Conf. 1997, Vancouver, Canada, Vol. 2, p. 1993
[3] http://www.crytur.cz/
[4] http://www.sbig.com/sbwhtmls/online.htm

Estimates of Absorbed Dose Rates around a Beam Dump at ELBE

B. Naumann[1]

Beam dumps will be used to aborb the electron beam energy of the radiation source ELBE. In the FEL cave it is planned to install the beam dump in front of a 3.6 m thick concrete wall and to shield it by iron and heavy concrete. The planned thickness of the iron layer in beam direction is about 30 cm resp. three tenth-value layer thicknesses of iron. For an axial symmetrically geometry (Fig. 1) the absorbed dose has been calculated using the particle transport code FLUKA [1]. The dose distribution in the described area for an electron beam with an energy of 50 MeV is shown in Fig. 2.

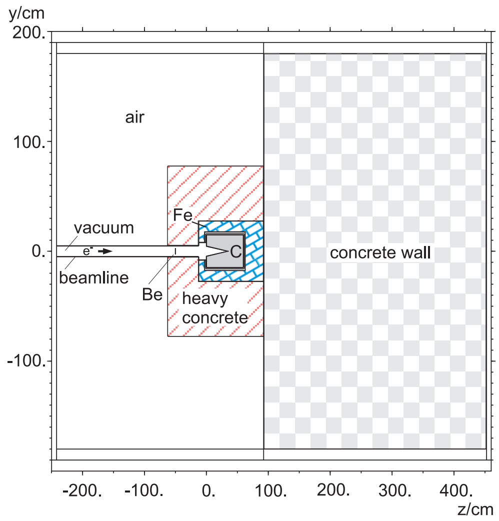

Fig. 1: *The placement of a graphite beam dump surrounded by iron and concrete shielding in front of a 3.6 m thick concrete wall.*

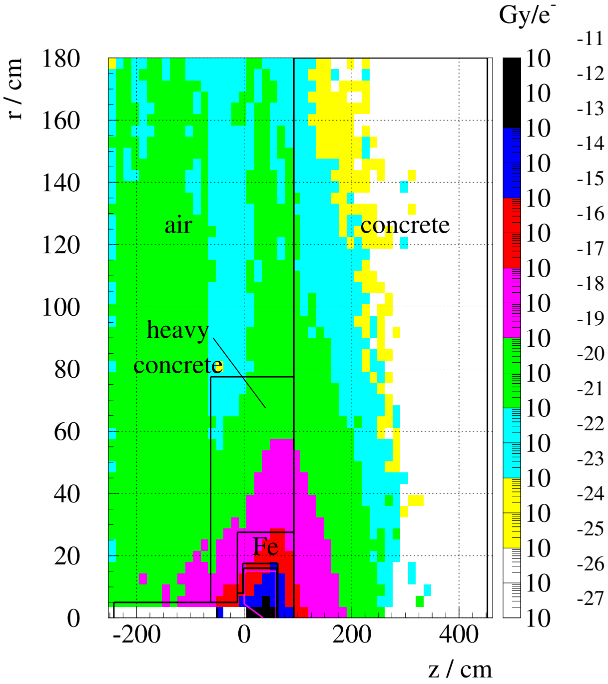

Fig. 2: *The dose distribution for a cylindrical geometry at an electron beam with 50 MeV energy.*

Assuming that the maximum dose is obtained along the beamline, the dose distribution into the inner radial section has been extracted from the dose distribution of Fig. 2. The dose distribution along the beamline inside the concrete wall (Fig. 3) has been calculated up to a depth of about 1 m with good statistics and the tenth-value layer thickness of the concrete has been obtained to 34.9 cm. This value is in a good agreement with data given in [2]. After passing the concrete wall the absorbed dose has been estimated approximately to $1.6 \cdot 10^{-27}$ Gy/e$^-$ and the dose rate to 0.04 μGy/h, which is two orders of magnitude lesser than the maximum value of dose rate for controlled areas $\dot{\mathrm{D}}_{max} = 5\,\mu$Gy/h.

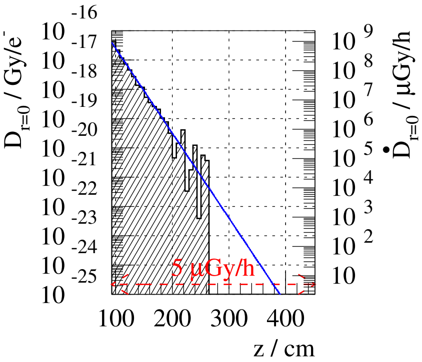

Fig. 3: *Dose and dose rate distributions along the beamline axis z inside the concrete wall.*

[1] *Institut für Kern- und Teilchenphysik, TU Dresden*

References

[1] A. Fasso et al., Proc. of the III Spec. Meeting on Shielding Aspects, Sendai (1997)61-74.

[2] Report NCRP-51, Radiation protection design guidelines, Washington (1977).

Calculations of the Power Dissipation and the Temperature Distribution in Beam Dumps at ELBE

B. Naumann[1], M. Werner[2]

The beam dumps for ELBE must be capable of absorbing an average beam power of 50 kW at an electron beam energy of 50 MeV. After passing a 500 μm thick beryllium foil the incident electron beam enters a purified graphite absorber ($\varrho = 1.7\,\mathrm{g/cm^3}$). The power dissipation for a first design of the beam dump was calculated using the particle transport code GEANT [1,2]. Further calculations have been performed with the transport code FLUKA [3], which makes possible to consider nuclear reactions like the (γ,n) process. Two geometrical shapes of the graphite core (V1, V2) have been compared with respect to the power dissipation and the temperature distribution. Version V1 corresponds to the first layout [1] with a radius of 15 cm and a cone-shaped hole of 35 cm depth. The power dissipation for V1 is shown in Fig. 1. After reducing of the radius to 10 cm, the implementation of a second cone-shaped hole at the entrance (10 cm deep) and the elongation of the first cone-shaped hole up to 45 cm, the power dissipation in this version V2 is more homogeneously distributed as shown in Fig. 2.

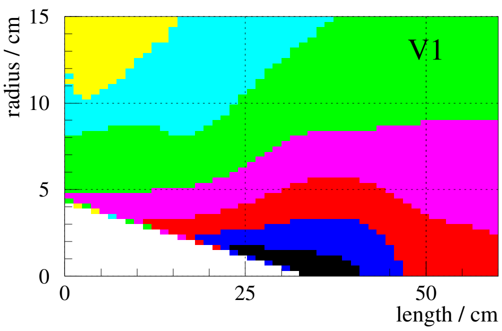

Fig. 1: *Power released in graphite core V1.*

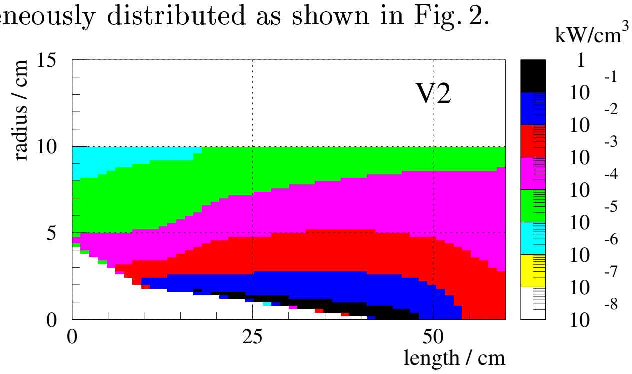

Fig. 2: *Power released in graphite core V2.*

On the base of the power dissipations the thermal loads were calculated for the two graphite cores using the Finite-Element-Code ANSYS [4]. The model comprises the heat transfer in the graphite and the radiation effect according to the Stefan Boltzman equation between the surface and the water cooling which surrounds the graphite core. The resulting temperature curves along the outer lines of the halfmodel for the two graphite cores are shown in Fig. 3. The maximum surface temperature at the centerline in V1 amounts to 2834 K and is near to the graphite sublimation temperature of 3300 K at a pressure of 5 mbar [1]. The improved geometry in V2 results in a smaller maximum surface temperature of 2256 K.

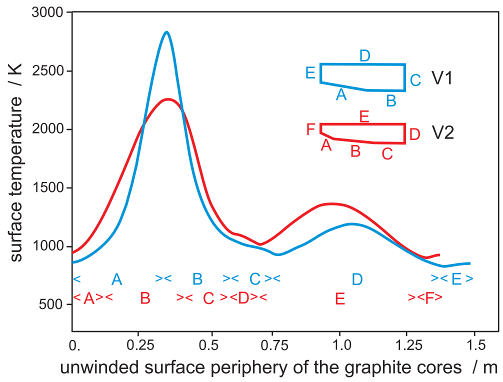

Fig. 3: *Profiles of the surface temperatures for two graphite core versions at an electron beam energy of 50 MeV.*

[1] *Institut für Kern- und Teilchenphysik, TU Dresden*
[2] *Institut für Sicherheitsforschung, FZ Rossendorf*

References

[1] B. Naumann et al., Strahlfänger für maximale Energien an ELBE, FZR Report FZR-267 (1999); Annual Report 1998/1999, FZR-271 (1999) 36.
[2] GEANT-Detector Description and Simulation Tool, CERN Program Library W5013 (1994).
[3] A. Fasso et al., Proc. of the III Spec. Meeting on Shielding Aspects, Sendai (1997) 61-74.
[4] ANSYS User's Manual for Rev. 5.6., Swansons Analysis Systems, Inc. (1999).

Field Measurements on the ELBE Undulator U27

P.Gippner, E. Grosse, W. Seidel, J. Pflüger[1], A. Schamlott, U. Wolf

In order to produce at ELBE an intense FEL radiation in the infrared region we shall install the undulator U27 which consists of two sections with a length of $0.98\,m$ each and a short region in between with three adjustable magnetic dipoles. Each section consists of $N_u = 34$ magnetic periods with a length of $\lambda_u = 27.3$ mm. The magnetic structures for both units were test modules for the TTF-Facility at DESY, Hamburg [1,2] and the carriages have been constructed and delivered by DANFYSIK. The fig. 1 shows the carriages before the magnets have been mounted. For optimization of the phase-matching of the two sections the distance between them is adjustable over a wide range by using a stepping motor.

The carriages are designed such that the gap of both sections can be varied independently. For special applications they can also be tapered individually, what should result in an increase of the extraction efficiency [3,4]. The undulator field was measured and tuned at HASYLAB (DESY) by means of the Hall probe shown in fig. 2.

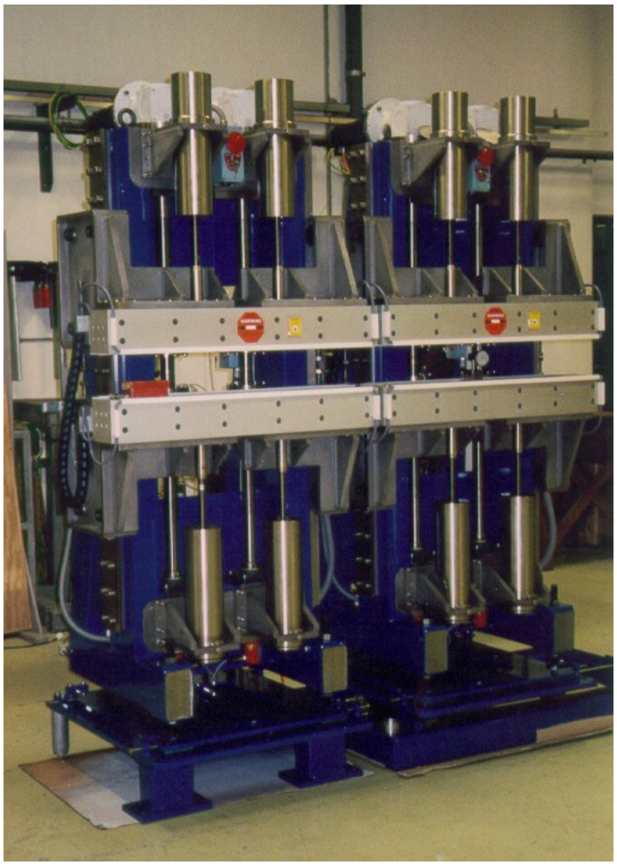

Fig. 1 *The undulator carriages with girders before mounting the magnetic structures.*

The probe is mounted on a goniometer with six degrees of freedom for right adjustment within the magnetic structures. The poles were tuned with the aim to get a minimum electron displacement at the exit sides of the modules as well as a peak field roughness lower than 0.4 %. As a result of the measurements the fig. 3 shows the field component $B_y(0,0,z)$ in the middle plane of both undulator units for a gap of $g = 12$ mm and a distance $d = 250$ mm between the sections (a) and the first integral over the measured field (b). The trajectory of a reference electron with an energy of $E = 20$ MeV in the wiggle plane is shown in part (c). Fig. 4 shows the magnetic field distribution $B_y(x,0,z_5)$ perpendicular to the electron beam at different gaps , where z_5 is the center of the 5th pole.

In order to make the gap variation more convenient we tried to design a "passive" undulator. Thereby the elongation of the electrons for a given energy should be nearly independent of the gap width, whereas the displacement Δ and the slope of the trajectory at the exit should be as small as possible. Corresponding calculations have been done with the code RADIA [5] and have already been reported [6]. However the fringe field turns out to be not absolutely passive against gap widening but causes a weak dependence of Δ on the gap. This can be corrected by coils mounted at the entrance sides of both sections and allowing to inject the electrons under a small angle relatively to the z-axis. Only weak magnetic fields of about 2 mT are necessary to keep the electrons within the optical mode.

Presently the influence of shimming on the fringe field is under investigation.

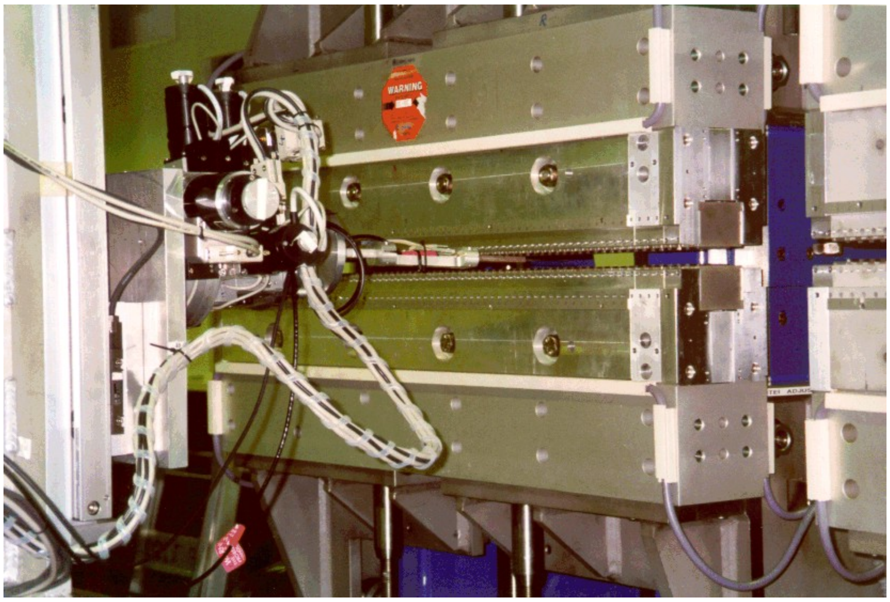

Fig. 2 *The Hall probe mounted on a goniometer for field measurements on the axis of one of the undulator sections.*

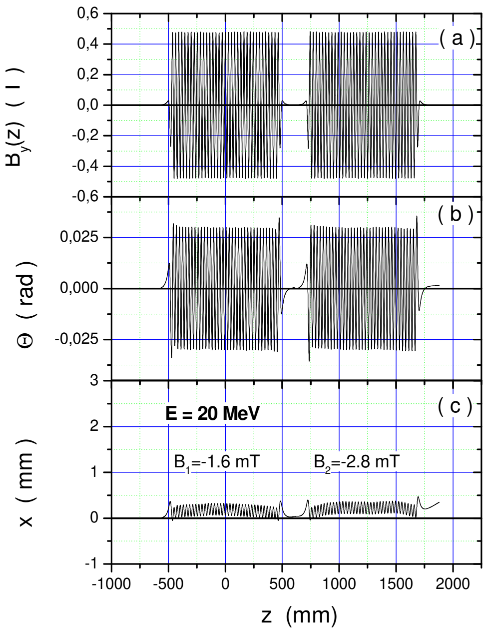

Fig. 3 *The field distribution $B_y(z)$ in the middle plane of the two undulator systems along the axis z for a gap width of $g = 12\,\mathrm{mm}$ (see text).*

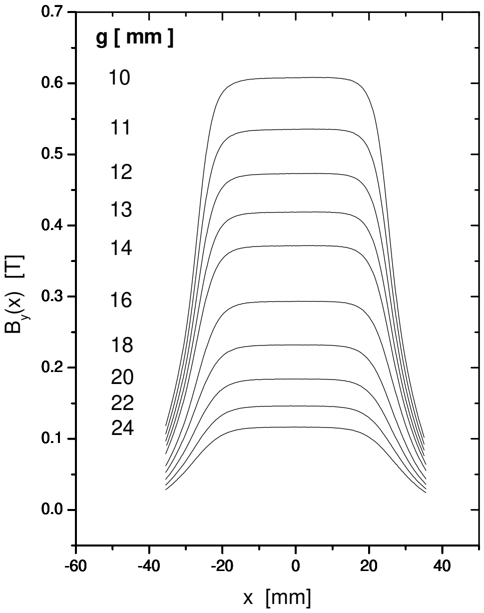

Fig. 4 *Magnetic field $B_y(x, 0, z_5)$ perpendicular to the electron beam at different gaps, where z_5 is the position of the 5th pole.*

[1] *HASYLAB at Deutsches Elektronen Synchrotron DESY, Hamburg*

References

[1] B. Faatz, J. Pflüger and Y.M. Nikitina, Nucl. Instr. Meth. A 375 (1996) 618
[2] Y.M. Nikitina and J. Pflüger, DESY Report TESLA-FEL 96-03
[3] E.L. Saldin, E.A. Schneidmiller and M.V. Yurkov, Phys. Lett. A 185 (1994) 469
[4] D. Jaroszynski et al., Phys. Rev. Lett. 72, 2387 (1994)
[5] P. Elleaume, O. Chubar and J. Chavanne, J. Synchr. Rad. 5 (1998) 481
[6] P. Gippner, W. Seidel and A. Schamlott, Annual Report 1998, FZR-271, p.16

Phase Matching of the Two Sections of the U27 Undulator

P. Gippner, J. Pflüger[1]

The U27 undulator consists of two 0.98 m long separate sub-systems which have individual mechanical drives for gap adjustment. Thus for variable gaps the radiation wavelength is changed and consequently the phasing between the two undulator systems has to be changed as well. This has to be done by properly choosing the electron flight path d between the two sections.
The optical phase in an undulator has been analyzed in detail by Walker[1]. It can be expressed by

$$\Psi(z) = \frac{2\pi}{\lambda_R}\left[\frac{z}{2\gamma^2} + \frac{\int^z dz'\Theta(z')^2}{2}\right]. \tag{1}$$

Here z is the coordinate along the beam axis, λ_R is the radiation wavelength, γ is the electron kinetic energy in units of its rest mass and Θ is the electrons deflection angle. The terms in the bracket have the following descriptive meaning: the first gives the contribution to the phase, if the electron travels just a distance z in free space, the second term represents the additional contribution due to the magnetic field. The function $\Theta(z)$ can be derived from $B_y(z)$ by

$$\Theta(z) = \frac{e}{\beta\gamma m_0 c}\int^z dz' B_y(z'). \tag{2}$$

Using the eqs. (1) and (2) the phasing of the two undulator sub-systems can be determined experimentally by measuring $B_y(z)$ along the axis of the entire undulator.
The phase on the poles in the second section varies with the distance d, which depends on the K-value and has to be chosen appropriately. Moreover, phase matching is obtained periodically after an increase of d by $\Delta d = \lambda_u(1 + \frac{1}{2}K^2)$. The deviation of the optical phase angle from its nominal value obtained for a perfect undulator is denoted by $\Delta\Psi(z)$. For a gap $g = 17\,mm$ measurements for $\Delta\Psi(z)$ are shown in fig. 1. The K-value for this case was 0.6688. The nominal phase deviation on the poles is nearly zero, only at the end poles before and after the interspace the phases deviate from zero. The proper choice of the distances d as functions of the K-value as determined experimentally is shown in fig. 2. Six different curves have been measured. They are shifted horizontally by $\Delta d = \lambda_u(1 + \frac{1}{2}K^2(g))$. These curves have to be used to choose phasing distances d_{ph} in dependence on the gap g.

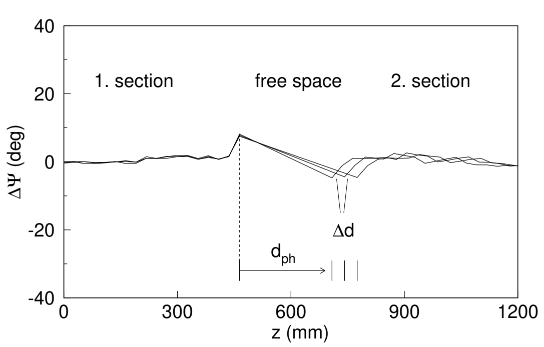

Fig. 1 *Phase differences $\Delta\Psi(z)$ for a gap g = 17 mm. The K-value is 0.6688. Three phasing distances d_{ph} are shown.*

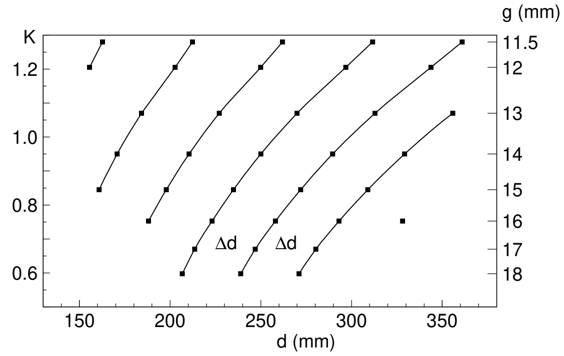

Fig. 2 *Phasing distances d_{ph} (points) between the two sections of U27. The right axis shows the gap widths g, for which the values d_{ph} have been found, the left axis shows the corresponding K-values in a linear scale.*

[1] *HASYLAB at Deutsches Elektronen Synchrotron DESY, Hamburg*

References

[1] R. P. Walker, Nucl. Instr. Meth. A 335 (1993) 328
[2] B. Faatz, J. Pflüger, P. Pierini, Nucl. Instr. Meth. A 375 (1996) 441-444

Tapering of the ELBE-Undulator U27

P. Gippner, E. Grosse, A. Schamlott, U. Wolf

If the FEL works with maximum power the energy factor γ of the electrons decreases by $\Delta\gamma = \gamma/2N_u$ (for the first harmonic) along the electron path due to the interaction of the electron beam with the electromagnetic field, where $N_u = 68$ is the total number of magnetic periods in the two undulator units [1]. The electron energy changes continuously from the undulator entrance to the exit leading to a resonance wavelength $\lambda(z)$ which depends on the coordinate z along the undulator

$$\lambda(z) = \frac{\lambda_u}{2\gamma^2(z)}(1 + \frac{1}{2}K^2). \tag{1}$$

Within a certain interval of λ this effect can be compensated by differentially increasing the gap, and hence decreasing the magnetic field along the undulator. To compensate the energy loss dγ by a reduction dB of the magnetic field one has to ensure

$$d\lambda = \frac{\partial\lambda}{\partial\gamma}d\gamma + \frac{\partial\lambda}{\partial K}dK = 0 \tag{2}$$

from which follows

$$\frac{dB}{B} = \frac{2 + K^2}{K^2}\frac{d\gamma}{\gamma}. \tag{3}$$

For hybrid undulators, the Halbach equation allows one to estimate the widening of the gap g needed for the variation dB of the field corresponding to equation (3). Figure 1 shows the effect of field tapering in both sections of the undulator U27, which would be used in a situation typical for high intensity lasing.

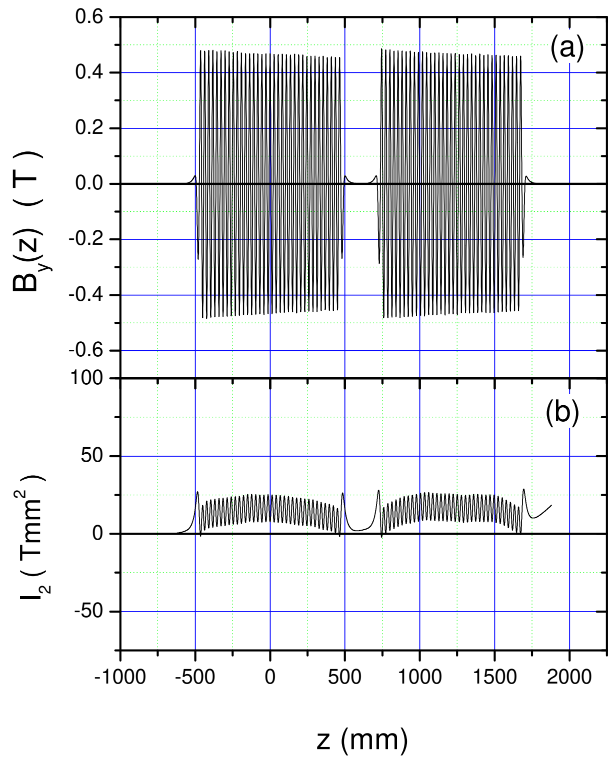

Fig. 1
(a) Measured field distribution $B_y(z)$ in the middle plane for a gap width $g = 12\,\mathrm{mm}$ and a tapering of 0.3 mm on the exits of both undulator sections.
(b) Second field integral I_2 of the undulator U27 as a function of the coordinate z. Within the scale used an influence of the tapering on the form of $I_2(z)$ is not noticeable. For conversion of I_2 in μm the formula $x[\mu m] = 300 \cdot I_2[T\,mm^2]/E[MeV]$ must be applied.

References

[1] P. Gippner, E. Grosse, W. Seidel, J. Pflüger, this Report

Application of the Pulsed Wire Technique to the Undulator U50

P. Gippner, U. Wolf, A. Schamlott, B. Rimarzig

In 2000 the ENEA undulator U50 was moved from Frascati to Dresden, but up to now we had no the possibility to control the magnetic structure of this equipment for damages originating by shocks during the transport. Corresponding measurements are normally made point by point using a Hall probe. Thereby great care must be taken for a precise mechanics and for the minimization of nonlinearities and calibration errors of the probe. Such measuring technique is not available at our institute. To find new irregularities of the magnetic field $B_y(z)$ arising from the transport we used the pulsed wire method [1, 2], which seems to be a much simpler technique than the Hall probe is. Parts of the equipment for this method and the software for data acquisition were delivered by ACCEL[1].

The pulsed wire method enables an in situ measurement of the first and second field integrals $I_1(z)$ and $I_2(z)$ of the magnetic structure depending on the current pulse form [1,2]. To measure these functions we used a CuBe wire with a diameter of $d = 50\,\mu$m and length of $L = 7500$ mm. The tension was produced by a mass of $m = 85$ g, resulting in a tensile force of $P = 0.83$ N and a tension of $T = 4.24 \cdot 10^4$ N/cm^2. In a first attempt an additional calibration magnet outside the undulator was not applied. The table 1 contains the electric parameters of the measurements.

Table 1

	I_1	I_2
current pulse length	$12\,\mu$s	20 ms
current pulse high	900 V	40 V
frequency	0.5 Hz	0.1 Hz

The measured integrals $I_1(z)$ and $I_2(z)$ in arbitrary units for a gap width of $g = 25$ mm are shown in fig. 1. The field component $B_y(z)$ is the derivative of $I_1(z)$ and was calculated by the data acquisition program.

The fig. 2 allows a comparison with the results obtained at ENEA with the Hall probe technique before the transport to the FZR was carried out. In general one can conclude that no additional field errors arised.

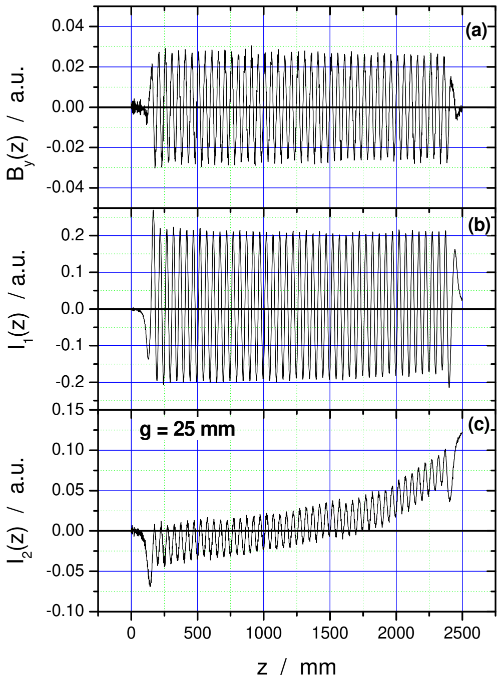

Fig. 1 *First field integral $I_1(z)$ (part b) and second field integral $I_2(z)$ (part c) measured with the pulsed wire method. The derivative $B_y(z)$ was not measured.*

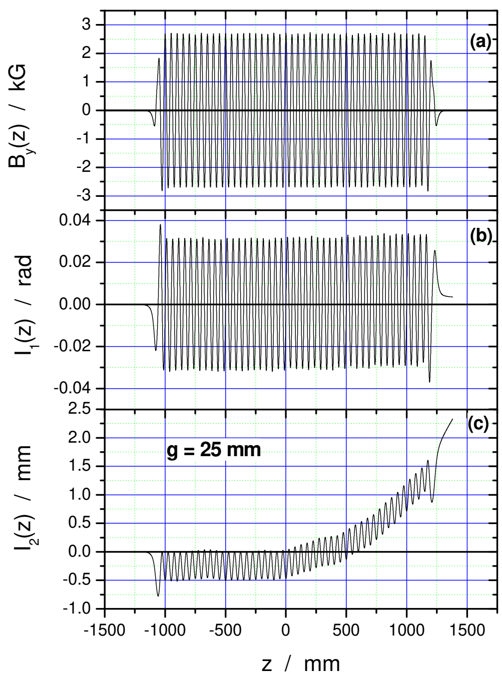

Fig. 2 *The field component $B_y(z)$ in the middle plane (a) measured with the Hall probe technique. The functions $I_1(z)$ and $I_2(z)$ are obtained by integration of $B_y(z)$.*

Finally, fig. 3 shows the second field integrals without and with an application of a homogeneous external field of $B = 3.3\,\mathrm{G}$ to correct the behaviour of this function. A bending effect can clearly be seen, which will help to guide the electron trajectories through the waist within the optical resonator. More quantitative investigations will be done in near future.

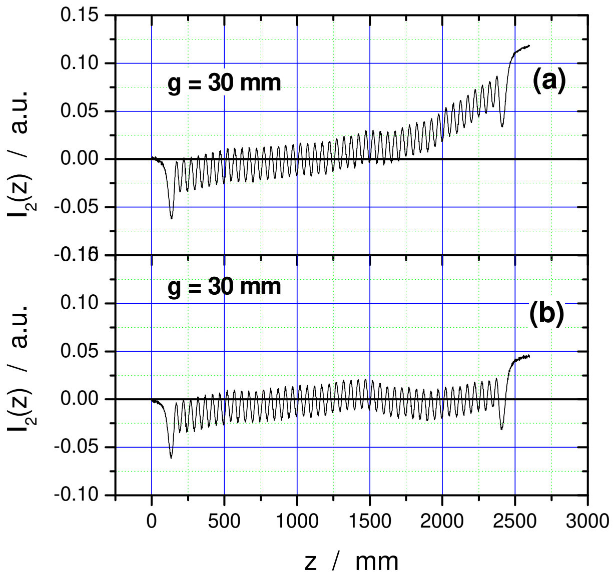

Fig. 3 *The integral $I_2(z)$ obtained by the pulsed wire method at a gap of $g = 30\,\mathrm{mm}$ without (a) and with an additional homogeneous field (b) of $B = 3.3\,\mathrm{G}$ in the exit part of the undulator.*

[1] *ACCEL Instruments GmbH, Bergisch-Gladbach*

References

[1] R.W. Warren, Nucl. Instr. Meth. A 272 (1988) 257

[2] A. Geisler, M. Ridder and Th. Schmidt, Delta-Rep. 94-8, University of Dortmund, Dept. of Accelerator Physics, unpublished

Magnet Field Errors of the ELBE Undulators and their Effect on the Laser Gain

P. Gippner, R. Wünsch

Two undulators (U27 and U50) are intended to be installed at the beam of ELBE to produce intense coherent radiation in the mid and far infrared range. To estimate the quality of the undulator we have measured the field strength B along the undulator axis z. In particular we consider the standard deviations σ_B and σ_Ψ of the magnetic field amplitude B and of the optical phase Ψ from their values in case of an ideal magnet. In an undulator with period length $\lambda_{\rm U}$ and rms parameter $K_{\rm rms}$, the optical phase is given by [1]

$$\Psi(t) \equiv k\,[ct - z(t)] = k\left[\frac{z}{2\gamma^2} + \frac{\int^z x'^2\,dz'}{2}\right] \qquad \left(k = \frac{2\pi}{\lambda}\right), \tag{4}$$

where $z(t)$ is the electron coordinate along the undulator axis and $x' \equiv dx/dz = e/(\gamma mc)\int^z dz'\,B_y(z')$ is the angle the electron makes with the z-axis in the transverse magnetic field B_y (m, $-e$ and γ denote mass, charge and energy of the electron; λ is the resonance wavelength $\lambda = (1 + K_{\rm rms}^2)\,\lambda_{\rm U}/2\gamma^2$). In an ideal planar undulator, the phase (1) oscillates uniformly with half the undulator period around a constant value if the resonance condition is fulfilled. For a realistic undulator, strength and period of the field scatter around the values in case of ideal field.

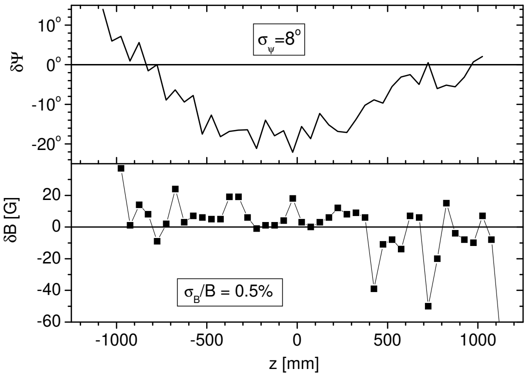

Fig. 1 *Deviations $\delta\Psi, \delta B$ of phase (1) and field amplitudes from their values in case of perfectly sinusoidal magnetic field as measured for the U50 undulator at the gap g=20 mm. $\sigma_{\Psi,B}$ denotes the variance of the corresponding quantity.*

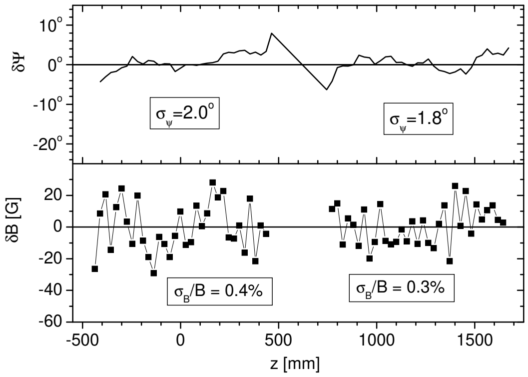

Fig. 2 *The same as in Fig. 1 for the two units of the U27 undulator at the gap g=14 mm. Similar results have been obtained for other gaps.*

Apart from the drift length between the two undulator units, where the electron does not interact with the field, the phase deviation for U27 (Fig. 2) is significantly smaller than for U50 (Fig. 1). That is the result of the meticulous tuning procedure applied to the U27 undulator.

The effect of the field errors on the lasing process has to be related to the electron energy spread σ_E. Both the deviations from their average values cause a line broadening σ_λ in the spontaneous emission spectrum which is also relevant for the degradation of the laser gain

$$\frac{\sigma_\lambda}{\lambda} = 2\frac{\sigma_E}{E} + \frac{2K_{\rm rms}^2}{1+K_{\rm rms}^2}\frac{\sigma_B}{B}. \tag{5}$$

For the ELBE beam ($\sigma_E \approx 90\,$keV) the first term in eq. (2) amounts to roughly 0.5% at E=40 MeV so that $\sigma_B/B \approx 0.5\%$ is only just small enough not further to reduce the laser gain considerably. On the other hand, the investigations of Bobbs et al. [2] have shown that a phase deviation smaller than 10^o does not significantly affect the laser gain.

References

[1] B. Faatz, J. Pflüger and P. Pierini, Nucl. Instr. Meth. A 375 (1996) 441-444

[2] B. L. Bobbs et al., Nucl. Instr. Meth. A 296 (1990) 574-578

The Magnetic Field Profile in the Wiggle Plane of the ELBE Undulators

C. A. J. van der Geer[1], P. Gippner, R. Wünsch

In an ideal undulator the magnetic field is assumed to be independent of the position in the wiggle plane (x-coordinate). In a real undulator consisting of finite magnets the field strength has a plateau in the center of the magnets ($x = 0$) and diminishes when moving toward their ends. The drop in the field strength defocuses the electron beam, i. e. electrons moving off the undulator axis and/or with a finite angle to it are deflected such that the beam size increases.

To study this effect we have measured and calculated the field profile in the wiggle plane of our undulators. We noticed a significant difference between the hybrid configuration (U27) and the Halbach construction (U50) even though their magnet blocks have the same width ($w = 50$ mm). Fig. 1 shows the measured field profiles for either configuration for a variety of undulator gaps. Generally, the hybrid magnetic configuration has a much more pronounced plateau than the Halbach construction has. At gaps below 10 mm, the first even has a small dip at $x = 0$, which is too small ($< 1\%$) to be visible on the scale of fig. 1

To investigate the effect on the electron beam we have calculated the average beam radius σ_x for either field configuration at the undulator exit for different gaps when starting with the same parallel beam of radius (0.4 mm) at the entrance. Fig. 2 clearly illustrates the pronounced defocusing effect in the Halbach undulator around a gap of 10 mm, in particular at lower energies. We also see the slight focusing action of the hybrid-type undulator at very small gaps. Note however that for a realistic simulation the beam divergence and the space charge have to be taken into account.

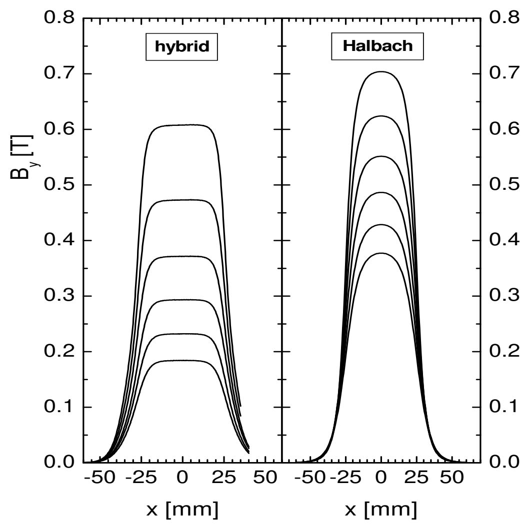

Fig. 1 *Measured transverse magnetic field profile of a hybrid undulator (left panel) in comparison to a Halbach construction (right panel) for the gaps $g = 10$, 12, 14, 16, 18 and 20 mm (from top to bottom). For the Halbach construction, only $g = 16$ and 20 mm have been measured. The other profiles have been calculated using the code RADIA [1] with parameters fitted to the measured profiles.*

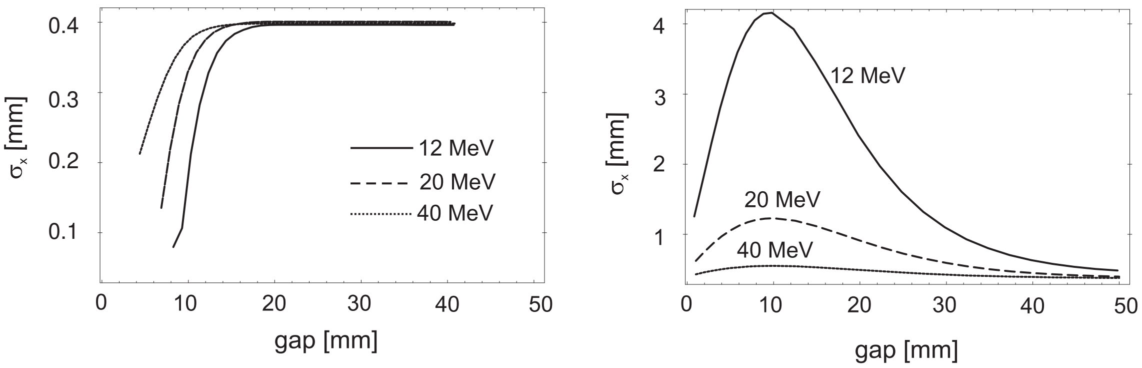

Fig. 2 *Beam radius (rms) σ_x in the wiggle plane after passing the undulator in either configuration as a function of the undulator gap for three different beam energies (indicated). Left panel: hybrid undulator (U27); right panel: Halbach construction (U50). $\sigma_x = 0.4$ mm at the entrance. Code GPT [2].*

[1] *FOM Institute for Plasma Physics Rijnhuizen, The Netherlands*

References

[1] P. Elleaume, O. Chubar and J. Chavanne, J. Syn. Rad. 5 (1998) 481-484

[2] Pulsar Physics, General Particle Tracer, http://www/pulsar.nl

Considerations on Cavity Loss Measurements for a Partial Waveguide Resonator FEL

M. Tecimer[1], E. Grosse, W. Seidel

A symmetric waveguide resonator configuration incorporating toroidal mirrors and a waveguide structure extending along the undulator section has been proposed for the 30 μm-150 μm far infrared FEL [1].

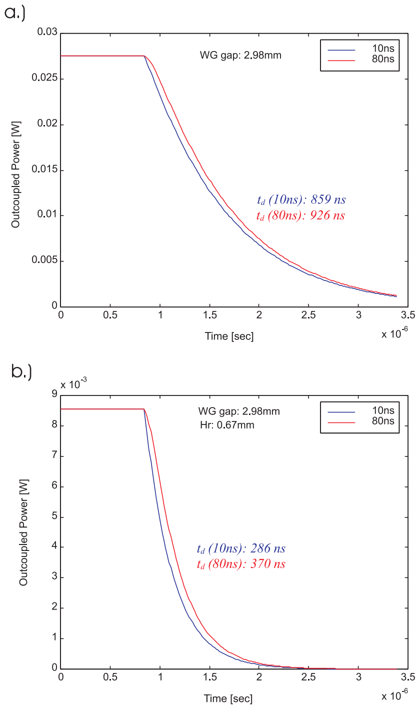

Fig. 1 *Simulated dependence of the outcoupled-power decay time on the pump-laser switching-off duration. In Fig.1b, additional losses due to a 1.35 mm diameter outcoupling hole has been taken into account leading to a shorter decay time.*

The use of toroidal resonator mirrors with optimized radius of curvatures helps to reduce cavity losses arising from the transition of the free space propagating mode into a wave guided one. The experimental study of the loss mechanism will be accomplished by means of a test resonator that is scaled down to the dimensions of an optical bench, according to the wavelength (10.6 μm) of the employed cw CO_2 seed-Laser. Measurements of the cavity ring down (CRD) time will determine the Q-Factor of the cavity and the associated resonator losses.

To be able to apply the CRD method, it is important to have the switching-off time of the pump laser being considerably shorter than the intracavity power decaying due to the loss mechanism (Fig. 1). In the planned experiments, after reaching steady-state, the power in the optical cavity will be switched-off within 80 ns using a acusto-optical modulator (AOM). The time dependence of the light intensity inside the cavity is then monitored by detection of the outcoupled light through the resonator mirror (Fig. 2) using a liquid-nitrogen cooled HgCdTe detector (MCT). A lens configuration located in front of the coupling mirror provides the necessary matching of the injected laser-mode profile into the lowest order hybrid mode excited in a parallel-plate waveguide.

In order to obtain an estimate for the losses and the associated cavity power decay time, a code has been developed based on the scalar diffraction theory [2]. It models the loss mechanism accounting for effects such as field outcoupling through the hole, mode conversion due to the hole and waveguide aperture, clipping-off the optical field at waveguide ends, transverse mode-matching of the injected laser-mode into hybrid modes, cross-coupling among the excited modes as well as temporal profile of the pump-laser decaying .

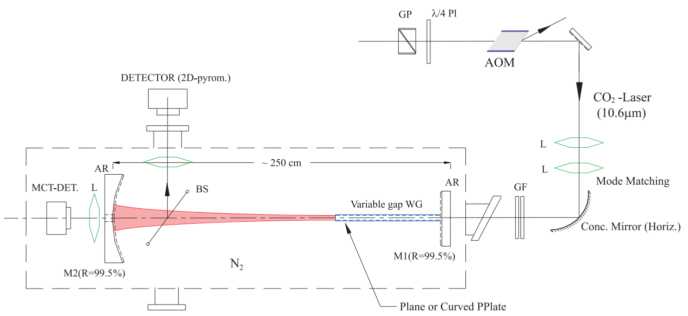

Fig. 2 *Schematic of the cavity ring down measurement setup.*

[1] *Tel Aviv University, Physical Electronics*

References

[1] M. Tecimer and R. Wünsch, this Report

[2] A. E. Siegman, Lasers, University Science Books, Sausalita CA, 1986

Losses in a Partial Waveguide Resonator of a FEL

M. Tecimer[1], R. Wünsch

The undulator U50 [1], which is a long-term loan from the ENEA Institute in Frascati, should at ELBE provide far infrared radiation up to roughly 150 μm. Already at 30 μm the transverse extension of the Gaussian mode in an open resonator is larger than allowed by the vacuum chamber located inside the undulator, leading to significant losses of optical power. To minimize these losses we propose a partially waveguided resonator 10 mm high that is guiding the wave along the undulator (240 cm) in the vertical dimension while the chamber is wide enough (40 mm) to allow the propagation of a Gaussian beam in horizontal direction. The currents induced by such a hybrid mode in the waveguide walls are small and the resulting ohmic losses are negligible [2]. Outside the undulator the vacuum chamber is large enough to ensure free propagation in either direction.

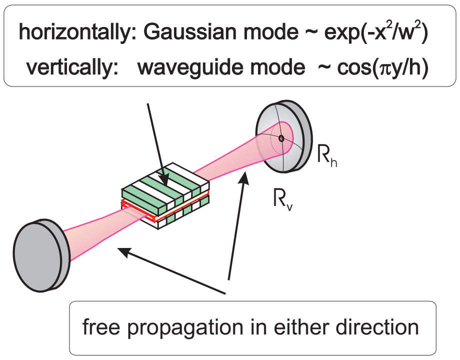

Fig. 1 *Optical beam in a resonator FEL with a waveguide mode inside the undulator and a Gaussian mode outside of it. The resonator mirrors have different radii of curvature R_h and R_v in the horizontal and vertical plane, respectively.*

Since the horizontal propagation of the optical beam is not affected by the waveguide, the horizontal radius of curvature R_h of the resonator mirrors is determined by the the gaussian optics. We choose a radius corresponding to a Rayleigh range z_R=1 m with a waist located at the center of the undulator.

The radius R_v in vertical direction determines the coupling of the waveguide mode inside the undulator with a free space mode outside of it. A detailed numerical analysis of mode coupling losses has been carried out using the code GLAD [3] and applying the diffraction theory based on the Huygens-Fresnel principle [4]. The results of computation (Fig. 2) show that at wavelengths larger than 30 μm the losses can be minimized by a mirror with a fixed radius of curvature R_v which corresponds to the distance D between mirror and waveguide exit. Below 30 μm the Fresnel number becomes so large that the appropriate radius of curvature depends strongly on the wavelength.

The simulated resonator characteristics will be investigated experimentally on a scaled down test resonator structure, excited by the radiation of a CO_2 laser at 10.6 μm. The Q-Factor of the cavity and the associated resonator losses will be then defined by means of a cavity ring down experiment.

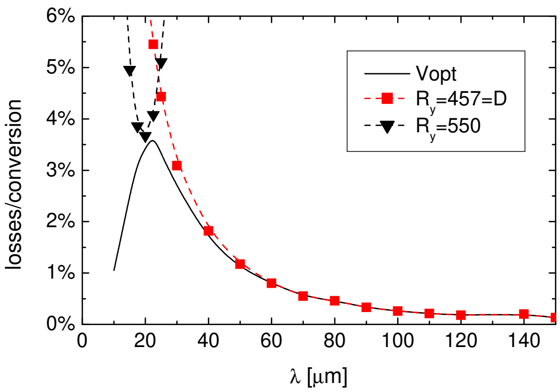

Fig. 2 *Losses of a single mode conversion in dependence on the wavelength λ of the radiation for two different radii of curvature R_v of the mirror. The full line shows the minimum losses which can be obtained with any mirror of constant curvature.*

[1] *Tel Aviv University, Physical Electronics*

References

[1] F. Ciocci et al., Nucl. Instr. Meth. A 250 (1986) 134-137
[2] L. Elias and J. Gallardo, Appl. Phys. B 31 (1983)
[3] G. Lawrence, GLAD, Applied Optics Research, Austin TX, USA
[4] A. E. Siegman, Lasers, University Science Books, Sausalito CA, 1986

Design of the Optical Cavity for a Far Infrared FEL with the ENEA Undulator for a Wavelength of 30 - 150 μm

B. Wustmann, A. Wolf

Design and construction of the optical Cavity of a far infrared FEL for the handling of long wavelengths is a great challenge. Tab. 1 shows the optical cavity and mirror parameters derived from the numerical simulations performed in [1] and [2] for the propagation of the optical mode in the 11,5 m long optical cavity using a partial waveguide within the undulator.

Table 1

Resonator length	11530.5 mm
Position shift of a mirror	2 mm
Stability of the mirror distance	1 μm
Distance resolution	< 0.5 μm
Increment	< 0.5 μm
Direction change hysteresis	< 0.5 μm
Angle error of the cavity mirror	< 5 μrad
Error of the mirror surface	2 μm
Horizontal mirror diameter	145 mm
Vertical mirror diameter	270 mm
Mirror thickness	25 mm
Horizontal radius of curvature	5995 mm $\pm$ 0.25%
Vertical radius of curvature	4585 mm $\pm$ 0.25%
Diameter of the outcoupling hole	6 mm
Waveguide heigth	10 mm $\pm$ 0.1 mm
Waveguide width	40 mm
Waveguide length	2360 mm
Waveguide surface roughness	1...2 μm

These parameters were determined by the following boundary conditions:
The partial waveguide within the undulator guides the optical mode in the vertical direction through the narrow 20 mm magnetic gap in form of a fundamental waveguide mode with cosine distribution. The optical mode in horizontal direction has a Gauss-shaped freely spreading mode form both within and outside of the waveguide.
Due to this hybrid structure and the different divergence of the optical mode in horizontal and vertical direction outside the waveguides so-called bifocal concave toric mirrors with an elliptical cross section have to be used.
As the outlet of the optical gap in the waveguide amounts to 10 mm, the strong beam divergence in vertical direction results in a necessary mirror diameter of 270 mm for a wavelength $\lambda = 150\mu$m.
The mirror chambers have a diameter of about 300 mm. In fig. 1 and 2 they are shown with the necessary assembly nipples for the diagnostic and servo units.
The outcoupling of the laser radiation is made by means of a centric 6mm hole in one of the cavity mirrors. Additionally a horizontal insertable scraper mirror [3] should be able to outcouple a variable part of the laser.
For the alignment of the magnetic axis of the undulator, the electron beam axis and the axis of the optical cavity three insertable Berillium viewscreens with a centric hole of 1 mm are used within the waveguide (fig. 3).
The production technology for the waveguide is being verified by practical attempts. The detail construction of the mirror chambers has started and the draft design and version comparison of the optical cavity have been finished.
The dimensions of the scraper mirror and its vibration-free mounting are open problems.

References

[1] R. Wünsch, FZR-276 (1999)
[2] M. Tecimer and R. Wünsch, Losses in a Partial Waveguide Resonator of a FEL, this Report
[3] R. Nagai et al., An Optical Resonator with Insertable Scraper Output Coupler for the JAERI Far Infrared Free Electron Laser, 22th Free Electron Laser Conference, Durham, North Carolina, August 13-18, 2000

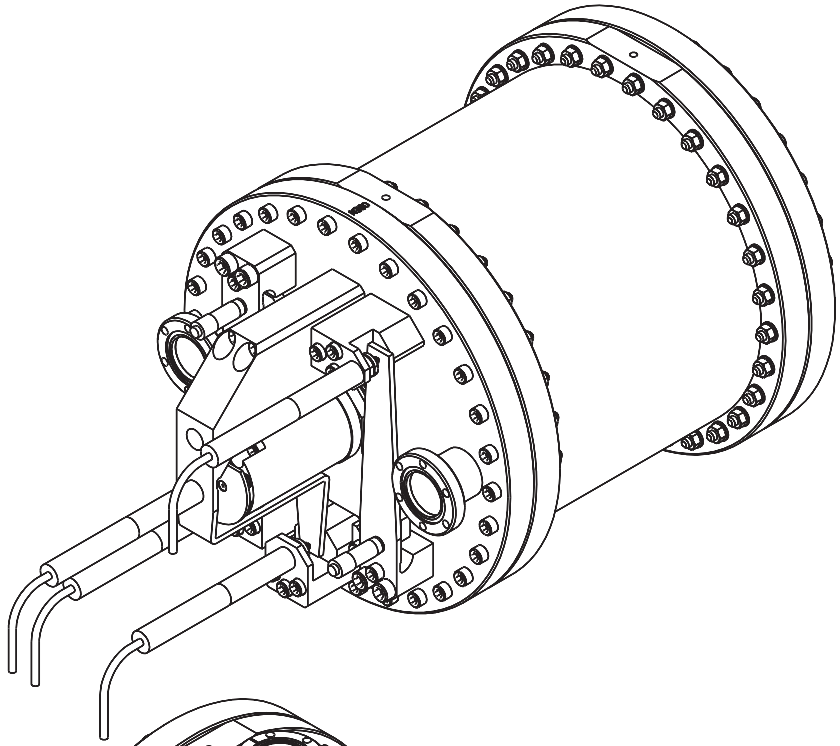

Fig. 1 *Mirror Chamber 1*

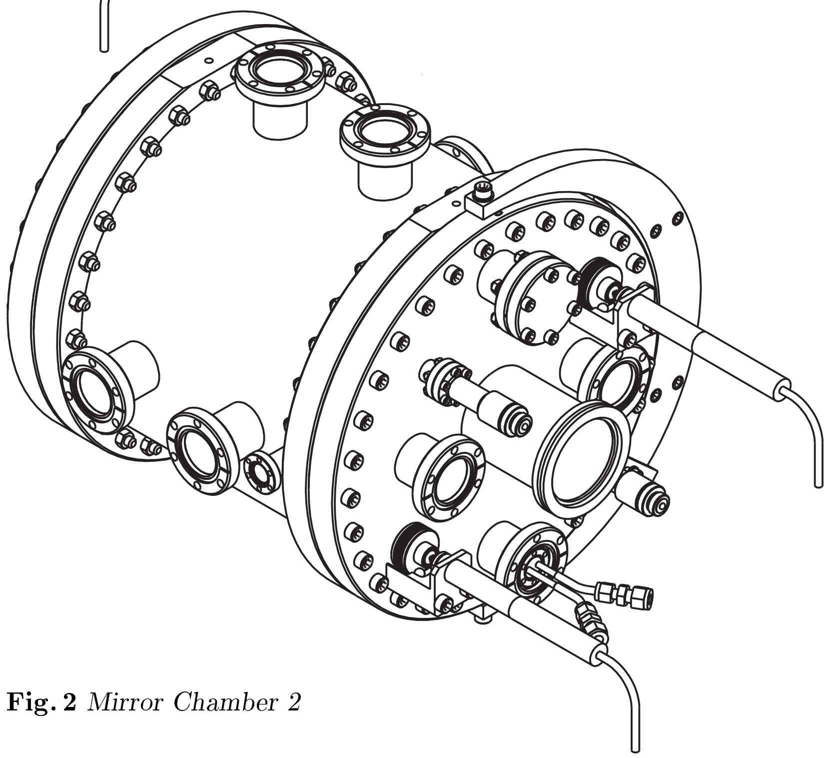

Fig. 2 *Mirror Chamber 2*

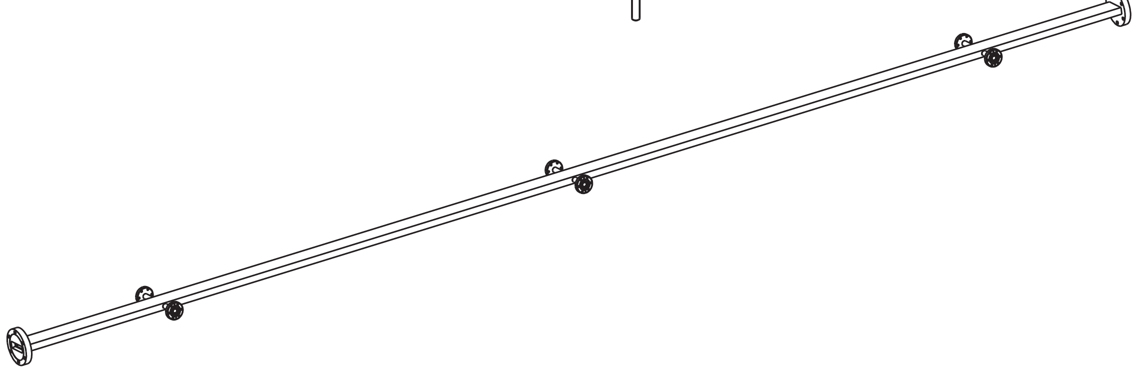

Fig. 3 *Wave Guide*

Infrared-Microspectroscopy of Environmental Samples

W. Seidel, A. Schamlott, D. Kalionska, K.H. Heise[1], R. Nicolai[1], J.-M. Ortega[2], F. Glotin[2], R. Prazeres[2]

The goal of this application of infrared radiation is the microspectroscopy of organic components and their heavy metal complexes in solid or liquid environmental samples.
The absorption bands due to the vibrational transitions are in the wavelength region of $\lambda = 2 - 200\,\mu$m $(5000 - 50\,cm^{-1})$. The absolute amounts of the components are very small. The concentration of solved organic components in environmental water samples is usually lower than 10^{-6} Mol/l. The conventional infrared spectrometry requires a particular sample preparation. Different measuring techniques are known, but the sensitivity and the position resolution are not satisfactory.
In order to improve the sensitivity of infrared measurements we are developing a thermo optical detection method based on the mirage effect [1]. A solid sample is periodically irradiated by a beam of monochromatic light produced by the free-electron laser (FEL) CLIO at Lure/Orsay in France. An absorption induces a temperature gradient which leads to an increase of the refractive index gradient. This deflects a probe beam (i. e. He-Ne laser) propagating along the surface of the sample (mirage effect). The periodic deflection of the probe beam is monitored by the use of a high resolution position detector placed at a suitable distance away from the illuminated sample. The magnitude of this periodic deflection can then be related to the absorption coefficient of the material under investigation. This results in an extremely high sensitivity (absorbances as low as 10^{-6} to 10^{-8} have been measured in the visible light by this method). We have carried out absorption measurements in the wavelength range from 9 μm up to 40 μm with different samples. In these measurements we could reproduce some features of the absorption of the samples, corresponding to the FTIR spectra. With the incident energy being modulated, the heat generation will show a corresponding time dependence. A temperature profile then develops in the sample via heat diffusion. For a heat source with a modulation frequency f the heat diffusion can be described by the thermal diffusion length

$$D = \sqrt{\frac{\kappa}{\pi \varrho C f}}$$

κ denotes the thermal conductivity, ϱ the material density and C the specific heat of the sample. Only heat generated within one thermal diffusion length will be able to reach the surface with an appreciable magnitude. For SiO_2 one finds D $\sim 1.5\,\mu$m for f = 1 MHz. This result means that if the signal is measured about 1 μs after the beginning of the laser pulse, the heat had time to diffuse only over a length shorter than 2 μm. Therefore, one can hope for a spatial resolution much smaller than the FEL wavelength, thus allowing eventually microspectrometry. In that case the He-Ne laser would have to be focused on a sufficiently small spot, which has not yet been done in the present, preliminary, experiments.
We started first resolution test experiments with synthetic samples in May and October 2000. For this runs we prepared samples with the IR absorption in a controlled manner. The pellets are made from KBr as matrix with homogeneous inclusions of interested materials (humic acid). Furthermore, we measured one natural sample of calcite containing humic acid inclusions.

We have carried out absorption measurements in the wavelength range from 9 μm up to 15 μm (1100 – 670 cm^{-1}). The average IR-power of CLIO was in the order of 1 W over the wavelength range. The laser time structure contains 10 μs trains (consist of short micropulses, which have a duration of < 10 ps and are separated by intervals of 16 ns) with 25 Hz repetition rate. For the measurement of the absorbance we have averaged the maximum deflection of the He-Ne laser beam over 20 macropulses at each wavelength. In different measurements we could reproduce the structure of the absorption spectra of the samples, corresponding to the FTIR spectra.

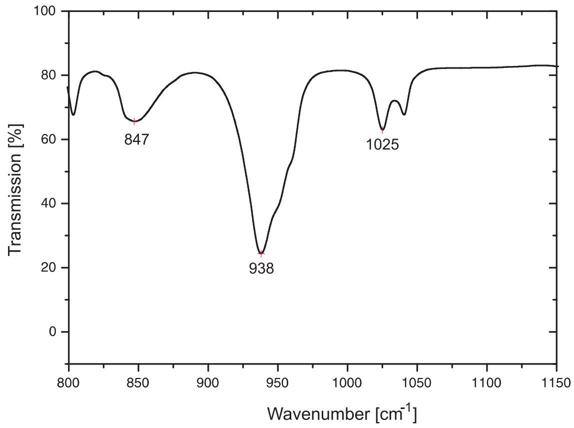

Fig. 1 *FTIR spectrum of the test sample (the substructure in the peak at 938 cm^{-1} is smeared out due to the reduced resolution of this measurement).*

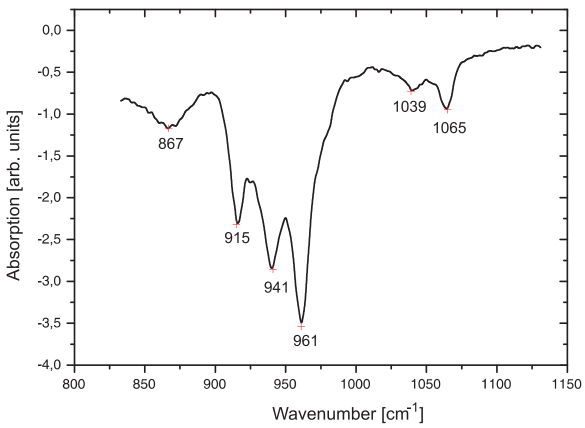

Fig. 2 *Spectrum obtained by the mirage effect at the CLIO FEL.*

Fig. 1 shows the FTIR-spectrum of a test sample (0.74 mg $UO_2\,(NO_3)_2\ \times 6\ H_2O$ in 300 mg KBr-pellet) measured with a Perkin-Elmer Mod 2000 spectrometer, the spectrum measured at the CLIO FEL is shown in fig. 2. The splitting of the wide absorption peak around 941 cm^{-1} into tree peaks was not observed in the samples with lower concentrations of nitrate and will be investigated more detailed in near future. In a next series of FEL experiments we would like to test this method at longer wavelength in order to show that it will be a good possibility for spectroscopic investigation with spatial resolution. Preliminary results have already been obtained on Teflon between 25 μm and 40 μm showing the applicability of the method at long wavelengths.

[1] *Institute of Radiochemistry*

[2] *LURE, Orsay, France*

References

[1] A.C. Boccara, D. Fournier, and J. Bodez, Appl. Phys. Lett. 36, 130 (1980)

Calculating the Spectral Distribution of Bremsstrahlung

A. Wagner, S. Fan, H. W. Barz, E. Grosse, R. Schwengner

One area of research of the new ELBE facility at the FZR will be devoted to nuclear spectroscopy studies by means of nuclear resonance fluorescence experiments using polarized photons and by means of photon-induced fission producing radioactive nuclei of interest. For these experiments detailed knowledge about the spectral distribution of photons from Bremsstrahlung production is mandatory. Therefore, three different approaches to determine the spectral distribution of photons emerging from a thin foil irradiated with electrons have been taken. Two calculations are based on Monte-Carlo simulations with commonly available software packages, GEANT [1] and EGS4 [2], and the third one is based on an analytical treatment in a quantum electrodynamics (QED) approach as described by Itzykson and Zuber [3]. Only the QED approach gives a result for the polarization of photons. All calculations have been done for 20 MeV and 30 MeV incident electron energy using a radiator thickness of 20 μm in the Monte-Carlo calculations. The QED spectrum has been scaled arbitrarily to match at 50% of the maximum photon energy. In order to limit the time needed for the simulations the low energy cutoff for the propagation of particles and photons in GEANT is set to 100 keV whereas it is set to 1.5 MeV for electrons and 100 keV for positrons and photons in the EGS4 calculations. Generally, the agreement between the different calculations is quite good and deviations mainly show up in the high-energy part of the spectra. Nevertheless, as shown in Fig. 2, EGS4 gives a better agreement to the QED calculations for photon energies close to the end-point as compared to GEANT. The GEANT calculation overestimates the spectra by at least 10% for the upper 10% of the spectra. The slight relative enhancement of both Monte-Carlo spectra for the low-energy part as shown in Fig. 2 indicates the influence of absorption inside the radiator which are neglected by the analytical treatment.

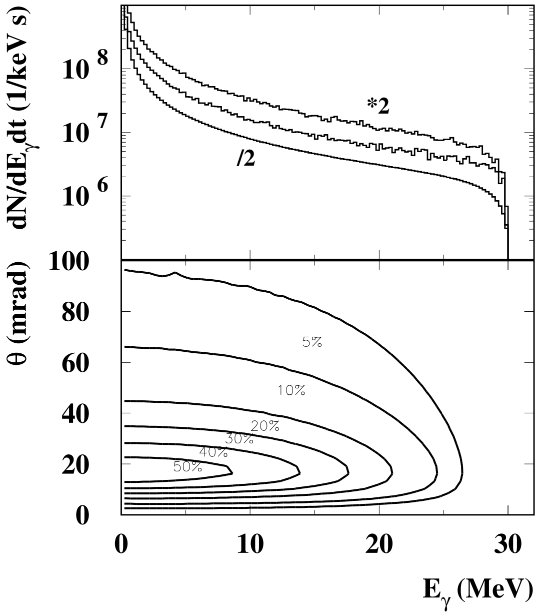

Fig. 1 *Upper part: Bremsstrahlung photon spectrum for a 20μm Aluminum radiator and incident electron energy of 30 MeV calculated by GEANT (middle), EGS4 (upper, multiplied by factor of 2), and QED (lower, divided by factor of 2). Lower part: Degree of polarization of Bremsstrahlung photons as function of photon energy and polar angle of observation for incident electrons of 30 MeV (QED).*

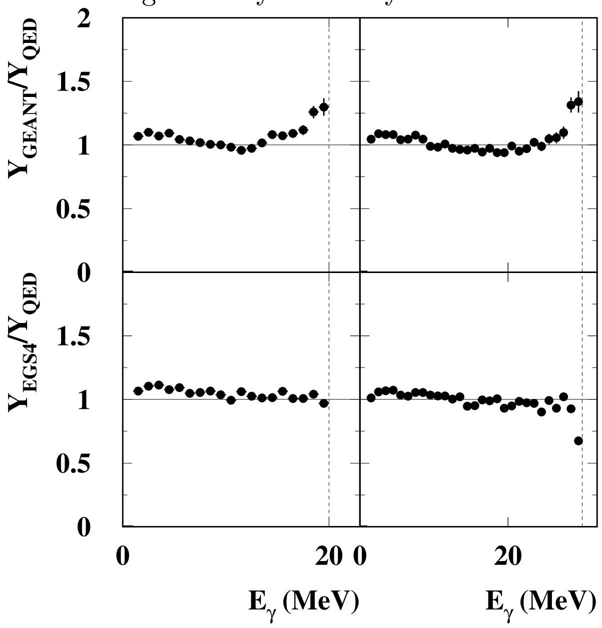

Fig. 2 *Energy dependence of the ratio of bremsstrahlung-spectra from GEANT (upper row) to the QED calculation and EGS4 (lower row) to the QED calculation for incident electron energies of 20 MeV (left column) and 30 MeV (right column).*

References

[1] CERN Program Library Long Writeup Q121, CERN, Geneva (CH), 1994
[2] The EGS4 code system, SLAC-R-265, UC-32, Stanford University
[3] C. Itzykson, J.-B. Zuber: Quantum Field Theory, McGraw-Hill, 1988

Postneutron Yield of Bremsstrahlung-Induced Fission of ^{238}U with an Endpoint Energy of 12 MeV

S. Fan, A. Wagner, E. Grosse

In order to examine the feasibility of studying neutron rich nuclei close to the astrophysical r-process path at ELBE we investigated the production cross sections of fission fragments from photo-induced fission. The isotopic fragment distribution from bremsstrahlung-induced fission of ^{238}U using bremsstrahlung from incident electron energies E_e can be written as

$$Y(Z/A) = \frac{N_i \int_0^{E_e} F_p(E) exp - \frac{(Z-Z_p(E(E_e)))^2}{2\sigma_Z^2} N(E(E_e))\sigma_F(E)dE}{\sqrt{2\pi}\sigma_Z \int_0^{E_e} N(E(E_e))\sigma_F(E)dE}$$

where the bremsstrahlung spectrum $N(E(E_e))$ was calculated using EGS4 [1], the photofission cross section σ_F was taken from Ref. [2]. Z_p denotes the most probable charge in a Gaussian distribution and was calculated using the Z_p model [3]. The width parameter σ_Z of the charge distribution from photofission of ^{238}U was found to be 0.34 [4], and N_i denotes the normalization parameter. The correction factor $F_p(E(E_e))$ for the proton odd-even effect is defined [4] as

$$F_p(E) = \frac{1+\delta_p}{1-\delta_p} \text{ for even Z}, \quad F_p(E) = \frac{1-\delta_p}{1+\delta_p} \text{ for odd Z with}$$

$$\delta_p = \frac{\int_0^{E_e} \delta_p^{mono}(E)N(E(E_e))\sigma_F(E)dE}{\int_0^{E_e} N(E(E_e))\sigma_F(E)dE}$$

where $\delta_p^{mono}(E)$ was deduced from experimental data[4].
Fig. 1 shows the postneutron mass distribution for the ^{238}U(γ, f) reaction with bremsstrahlung from 12 MeV electrons [5]. Fig.2 depicts the elemental mass distribution and Fig.3 shows the isotopic distribution of postneutron fission fragments (colored), nuclei with known half-lifes are shown as open boxes, stable nuclei are shown as filled boxes. Also drawn is the limit of nuclei with mean lifetimes against β-decay of more than 43 ms from theoretical predictions by Moeller [6].

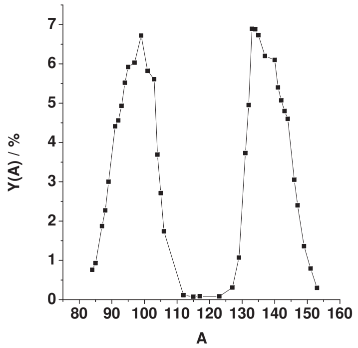

Fig. 1 *Postneutron mass distribution for ^{238}U(γ, f) reactions with bremsstrahlung from 12 MeV electrons [5].*

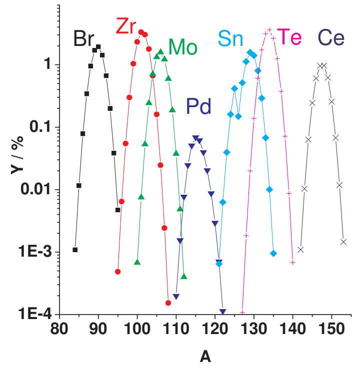

Fig. 2 *Elemental mass distribution (conditions as for Fig. 1).*

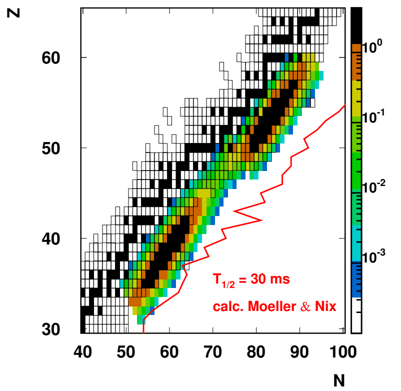

Fig. 3 *Isotopic distribution of fission fragments (colored). The contour line for expected half-lifes of 30 ms from theoretical calculations [6] is shown in red.*

References

[1] W.R. Nelson et al., SLAC-Report-265 (1985).
[2] B.L. Berman et al., Phys. Rev. C 21 (1980) 1215.
[3] R.K. Gupta et al., Phys. Rev. C 30 (1984) 395.
[4] K. Persyn et al., Nucl. Phys. A 620 (1997) 171.
[5] E. Jacobs et al., Phys. Rev. C 21 (1980) 237.
[6] P. Moeller et al., Atomic Data Nucl. Data Tables 66 (1997) 131-343.

A Beam Dump for Energetic Photons

A. Wagner, F. Dönau, E. Grosse, L. Käubler, K.-D. Schilling, R. Schwengner, W. Schulze

Nuclear spectroscopy studies at the new ELBE facility will make use of energetic photons from Bremsstrahlung production. In order to minimize the background from scattered photons the secondary photon beam has to be removed after passing through the experiment's target. Several different solutions have been studied by thorough Monte-Carlo simulations using the GEANT [1] program package. As a result, the configuration shown in Fig. 1 gives the minimal backscattering of photons towards the target area. It consists of a cylindrical inner absorber made from Polyethylene (PE) with a diameter of 80 cm and a length of 70 cm. This inner absorber is surrounded by a lead shielding with a thickness of 20 cm in axial and 10 cm in radial direction.

The selection of a low-density material like PE appears disadvantageous since it results in a large setup. Nevertheless, the high neutron production threshold and low (γ, n) cross section of 18.7 MeV for Carbon (for the most abundant isotope C-12) clearly favours PE as compared to lead. Moreover, Compton backscattering of photons for PE is reduced as compared to water by the lower mean atomic number density in PE. This lower atomic number of PE additionally lowers pair production and subsequently positron annihilation photons.

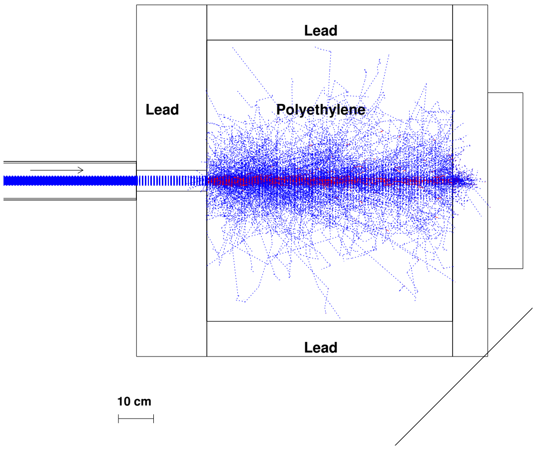

Fig. 1 *Simulated photon propagation of 20 MeV photons inside the photon beam dump. The photon beam is impinging from the left. Blue lines indicate photons, red lines indicate electrons.*

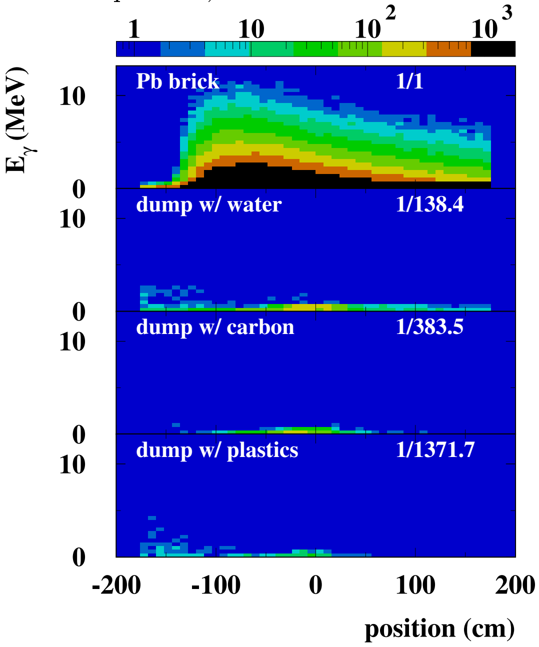

Fig. 2 *Spectral (ordinate) and position distribution (abscissa) of photons emerging from the photon beam dump and crossing a plane tilted by an angle of $\pi/4$ with respect to the photon beam. Different setups for the internal absorber of the beam dump are indicated with the integrated yield normalized to the first alternative featuring simply a lead brick at the end of the beam pipe. Different intensities follow a logarithmically scaled geographical colour map as shown on top.*

isotope	abundance	S_n (MeV)
H-2	0.02 %	2.22
C-12	98.9 %	18.7
C-13	1.1 %	4.95
O-16	99.8 %	15.7
O-17	0.04 %	4.14
O-18	0.2 %	8.04
Pb-204	1.4 %	8.39
Pb-206	24.1 %	8.09
Pb-207	22.1 %	6.74
Pb-208	52.4 %	7.37

Table 1 *Natural abundances and one-neutron separation energies for different isotopes used in the calculations.*

References

[1] CERN Program Library Long Writeup Q121, CERN, Geneva (CH), 1994

Optimization of a Quasi-Monochromatic X-ray Source for Cell Irradiations [B]

W. Neubert, W. Enghardt, U. Lehnert, B. Naumann, A. Panteleeva, J. Pawelke

Among the various secondary radiation sources proposed for the superconducting electron linear accelerator ELBE we consider the realization of an X-ray source for radiobiological investigations. For measuring relative biological effectivenesses of photons ($E_x \simeq 10 \div 100$ keV) by cell survival studies a channeling X-ray source is being developed. However, the quasi-monochromatic channeling radiation (CR) is contaminated by bremsstrahlung, which results both from the crystal and from the interaction of scattered electrons with the beam tube. Furthermore, neutrons are produced since the photon energy exceeds the threshold for photo-neutron reactions.

The beam line from the accelerator hall to the radiation physics cave was designed for a dispersion-free beam transport with minimal loss using the PARMELA code [1]. The system delivers an electron beam with $3\,\pi$ mm mrad normalized transverse emittance to the target crystal at focal spot diameters ranging from 4 mm to less than 1 mm. These parameters of the incident beam are chosen to meet the channeling condition. The channeling radiation yield was analytically calculated using the dipole approximation [2] for 20 MeV electron channeling along the (110) plane of a 100 μm thick diamond crystal. The maximum energies of channeling radiation emitted in forward direction are 17.1 keV (2$\rightarrow$1 transition) and 29.9 keV (1$\rightarrow$0 transition). But the interaction of the electron beam with the target strongly increases the beam divergence leading to collisions of electrons with beam line elements (Fig. 1). This causes a considerable bremsstrahlung background that may influence the radiobiological measurements, while the background contribution originating from the beam delivery to the target is negligible. Therefore, the complete setup downstream of the target crystal has been taken into account in GEANT [3] simulations as displayed in Fig. 1. For background calculations the electron beam was started at 1 cm in front of the carbon target that simulates the diamond crystal. The input (electron momentum distribution) was taken from the beam transport calculations. Multiple scattering in the target was found to be the dominating process which determines the beam divergence. Initially, the background calculations assumed a configuration with a distance of 123 cm between the crystal and the center of the dipole magnet which separates the electron beam from the photons. The full beam transport without consideration of electron scattering favours this solution but the electron tracking by GEANT shows too much bremsstrahlung production at the entrance of the dipole magnet. A significant reduction of the bremsstrahlung background in the GEANT simulations was achieved by increasing the beam tube diameters from 40 to 63 mm and the gap of the magnet from 60 to 90 mm. This way, the bremsstrahlung could be reduced to the level of the unavoidable contribution from the target. Secondary neutron production from these components has been treated by multiplying the bremsstrahlung photon

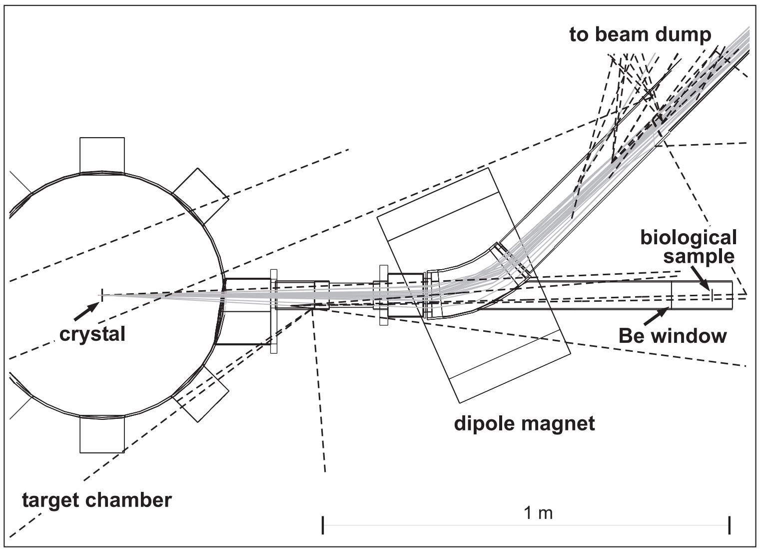

Fig. 1 *Top view of the channeling radiation source with tracks of electrons (grey) and photons (dashed).*

distribution with photo-neutron cross sections using the method described in [4]. In the optimized layout, the contamination of the X-ray dose delivered to the cell layer by neutrons is expected to be less than 1 %. The biological sample is assumed to consist of a monolayer of fibroblast cells (4 μm thick) placed on a 10 μm cellulose membrane and covered with a 8 mm thick medium layer. Fig. 2 shows the dose distribution in this sample produced by the photon beam after passing a 100 μm Be vacuum window calculated with the EGS 4 code [5]. We studied both tracking and energy deposition in such thin layers. A thickness greater than 1 μm was found to be necessary to perform dose calculations with EGS 4 in the photon energy range from 1.5 keV to 30 keV. The dose provided by the discrete channeling lines exceeds the bremsstrahlung background by at least one order of magnitude. But the integral dose of the bremsstrahlung is comparable to that of the channeling radiation. The introduction of an additional 70 μm Al absorber allows to reduce the low energy bremstrahlung contribution below 10 keV. It shows, however, that energy differential precision measurements of doses in biological samples require monochromatization of the photon beam, e.g. by reflection at a curved pyrolytic graphite crystal.

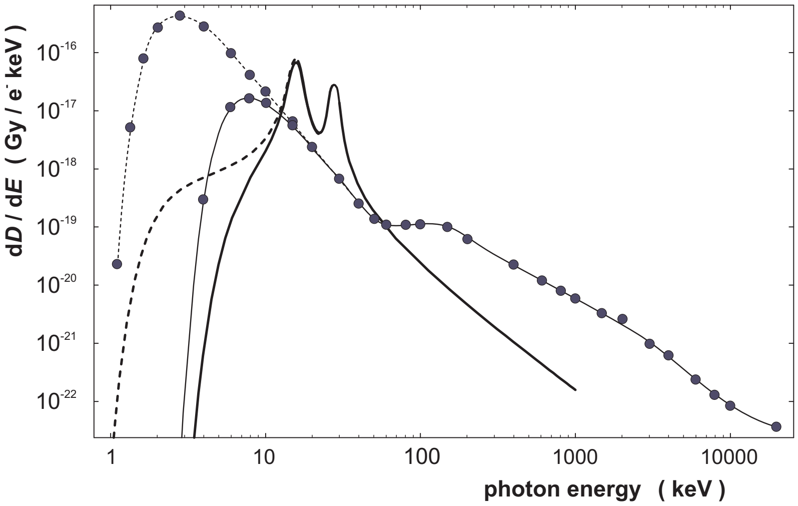

Fig. 2 *Dose distributions obtained by EGS 4 simulations for the described biological sample irradiated by bremsstrahlung (dots) and channeling radiation (thick line). The dotted and dashed lines are the corresponding calculations without the 70 μm Al absorber.*

Table 1 *Expected doses in the biological sample.*

Photon energy	Dose in 10^{-16} Gy / e^- with 100 μm Be window	with additional 70 μm Al absorber
1...10 keV background	13.00	0.70
10...100 keV background	1.04	0.86
$\geq$ 100 keV background	0.29	0.29
17 keV CR line	3.23	2.82
29 keV CR line	1.53	1.49

References

[1] L.M. Young, Los Alamos National Laboratory LA-UR-96-1835 (1996)
[2] M. Kumakhov and R. Wedell, Radiation of Relativistic Light Particles during Interaction with Single Crystals (Akademie-Verlag, Berlin 1991)
[3] GEANT-Detector Description and Simulation Tool, CERN Program Library W5013
[4] B. Naumann et al., Report FZR-267, Dresden (1999)
[5] W.R. Nelson et al., The EGS 4 code system, SLAC-Report-265 (1985)

Channeling in an Ultrasonic Superlattice [W,S]

L. Sh. Grigoryan[1], W. Wagner

A quantum mechanical description of channeling under the influence of ultrasound (US) excited in a single crystal has been developed [1–2]. It was shown that a resonant interaction between a longitudinal standing ultrasonic wave and planar or axially channeled relativistic charged particles can take place if the frequency of US approaches some critical value. This value corresponds to the energy difference between two neighbouring states a and b of transverse motion. The quantum numbers N of these states obey the selection rules $\mid N_a - N_b \mid = 1, 2, 3...$ for axial and $\mid N_a - N_b \mid = 2, 4, 6...$ for planar channeling.
The frequency of US necessary for resonance reads

$$\nu_n^* = \frac{v_s}{c} \frac{\mid \varepsilon_a - \varepsilon_b \mid}{n\, h}$$

where ε denotes the corresponding energy level of the channeled particle and v_s the velocity of US inside the crystal. Since the effect resembles a parametric resonance, an integer $n = 1, 2...$ appears in the denominator of the formula. This is of great practical importance because it opens the possibility of resonant interaction even at frequencies ν_s lower than typically 10 GHz for $n = 1$. At the same amplitude of crystal potential modulation, higher values of n, of course, diminish the effect of US.
Probability distributions of a planar channeled electron are shown in Figs. 1 and 2 versus the dimensionless coordinates $X = \alpha x$ and $Z = k_s z$ where the spatial coordinate z is chosen along the channeling direction, x is the transversal one, α denotes a scaling parameter of the crystal potential and k_s is the wave number of US. The only difference between the two figures consists in the US-frequency. At resonance (Fig. 1) US strongly mixes the corresponding channeling states a and b. Even a slight deviation of ν_s from the resonant value ν_1^* (Fig. 2) results in an abrupt reduction of the influence of US on the state of the channeled particle.

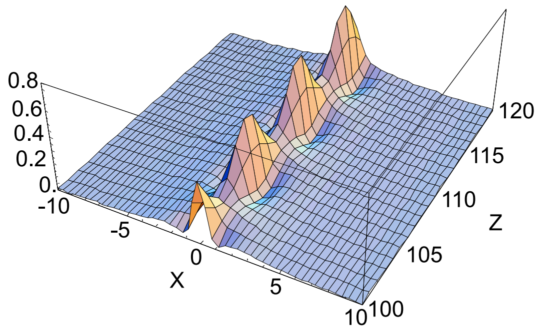

Fig. 1 *Probability distribution $P(X, Z)$ of a planar channeled electron at resonance ($\nu_s = \nu_1^*$).*

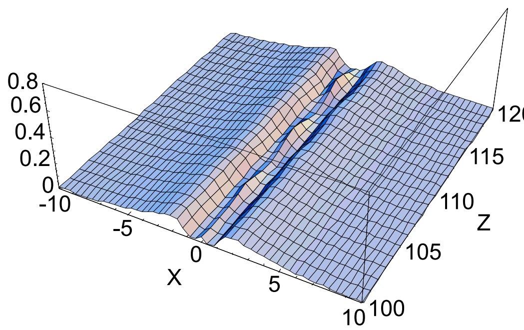

Fig. 2 *The same as in Fig. 1 but slightly out of resonance ($\nu_s = 0.95\, \nu_1^*$).*

[1] *Institute of Applied Problems in Physics, NAS Yerevan, Armenia*

References

[1] L.Sh. Grigoryan et al., Rad. Eff. & Def. in Sol. 152 (2000) 225; ibid. p. 269
[2] L.Sh. Grigoryan et al., Rad. Eff. & Def. in Sol. 153 (2000) 13

Mechanism of Channeling Radiation Stimulation by Ultrasound [W,S]

L. Sh. Grigoryan[1], W. Wagner

The interaction of a channeled relativistic charged particle with a standing ultrasonic wave excited in a single crystal leads to the splitting of the projection of its momentum in the channeling direction $(z) : p_z \Rightarrow \ (p_z - \hbar\, k_s\,,\, p_z\,,\, p_z + \hbar\, k_s)$. Here $\hbar\, k_s$ denotes the momentum associated with an acoustic phonon. The wave function of the channeled particle then represents a superposition of three plane waves with the phases $(p_z - \nu\, \hbar\, k_s)\, z/\hbar\ ,\ \nu = 0, \pm 1$.

Theoretical considerations on the influence of ultrasound (US) on channeling [1] formally predict the occurrence of additional radiative transitions which may amplify the total intensity of channeling radiation (CR). The mechanism of this effect instantly becomes reasonable from the following graphical treatment of CR.

Fig. 1 schematically illustrates the dispersion relation [2] $E = c\,\sqrt{m^2c^2 + p_z^2} + \varepsilon_N$ of a channeled particle for three stationary states $(N\ =\ 1,\, 2,\, 3)$ of transverse motion with the energy levels ε_N. Because of $E \gg \mid \varepsilon_N \mid$ the slope of these curves $\partial E/\partial p_z \approx v_z$ is determined by the particle velocity (v_z). By applying $\Delta E/\Delta p_z$ for the triangles CBD and CBA the known formula for the energy of CR emitted under an angle θ due to the transition AC :

$$\hbar\omega = \frac{\varepsilon_2 - \varepsilon_1}{1 - \beta\cos\theta}\ ,\ \beta = v_z/c$$

can directly be obtained from the ratio of these two expressions. In an analogous way, from the triangles GBA and GBF, one can for instance derive the adequate equation for an inverse transition AG accompanied with the emission of an acoustic phonon :

$$\hbar\omega = \frac{\varepsilon_2 - \varepsilon_3 - \nu\, c\, \hbar\, k_s}{1 - \beta\cos\theta}\ ,\ \nu = -1\ ,\ c\hbar k_s > \mid \varepsilon_2 - \varepsilon_3 \mid .$$

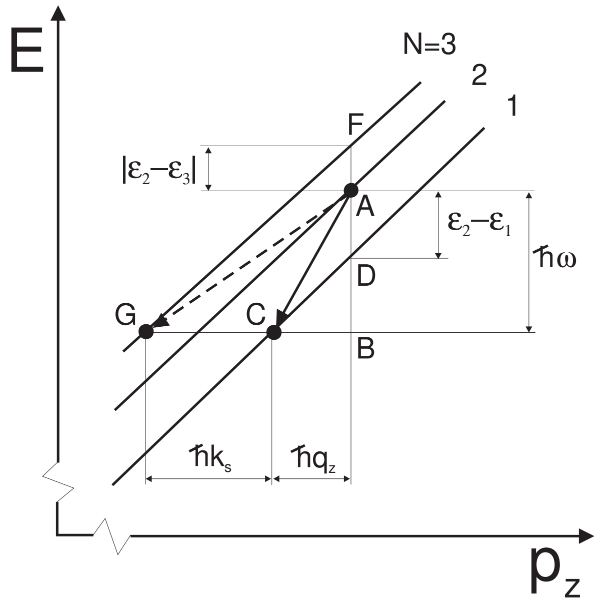

Fig. 1 *Schematic dispersion curves with two transitions (arrows) of a channeled particle.* $\hbar q_z = \hbar q\cos\theta$ *denotes the projection of the photon momentum* $q = \omega/c$ *onto the channeling direction.*

After such a *radiative* transition the channeled particle occupies a state with *larger* transverse energy; i.e. a CR-photon was emitted together with an acoustic phonon, and the quantum number N is increased.

Since in general $\nu = 0, \pm 1$ [1], the direct $(\varepsilon_i > \varepsilon_f)$ as well as inverse $(\varepsilon_i < \varepsilon_f)$ radiative transitions associated with the emission or absorption of an acoustic phonon are induced *additionally* to such with $\nu = 0$ which are not influenced by US. Consequently, US enables the channeled particle to emit multiple CR-photons during its traverse through the acoustically excited crystal that should result in an increase of the CR intensity.

[1] *Institute of Applied Problems in Physics, NAS Yerevan, Armenia*

References

[1] L.Sh. Grigoryan et al., Rad. Eff. & Def. in Sol. 152 (2000) 225; ibid. p. 269; vol. 153 (2000) p. 13
[2] J.O. Kephart, Stanford University, Ph.D. thesis (1987)